PMPCA mutations cause abnormal mitochondrial protein processing in patients with non-progressive cerebellar ataxia

Rebekah Jobling, Mirna Assoum, Oleksandr Gakh, Susan Blaser, Julian A Raiman, Cyril Mignot, Emmanuel Roze, Alexandra Durr, Alexis Brice, Nicolas Lévy, et al.

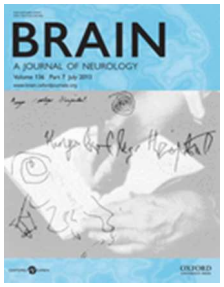

PMPCA Mutations cause Abnormal Mitochondrial Protein Processing in Patients with Non-Progressive Cerebellar Ataxia

Journal:	*Brain*
Manuscript ID:	BRAIN-2014-01750.R1
Manuscript Type:	Original Article
Date Submitted by the Author:	09-Dec-2014
Complete List of Authors:	Jobling, Rebekah; The Hospital for Sick Children, Assoum, Mirna; Aix Marseille Université, Gakh, Oleksandr; Mayo Clinic, Blaser, S; The Hospital for Sick Children, Raiman, Julian; The Hospital for Sick Children, Mignot, Cyril; APHP, Groupe Hospitalier Pitié Salpêtrière, Unité Fonctionnelle de Génétique Médicale Roze, Emmanuel; APHP, Groupe Hospitalier Pitié-Salpêtrière, Durr, Alexandra; Pitié-Salpêtrière Hospital, Department of Genetics and Cytogenetics Brice, Alexis; INSERM U679, Hôpital Pitié-Salpêtrière; Département de Génétique, Cytogénétique et Embryologie, Hôpital Pitié-Salpêtrière Lévy, Nicolas; Inserm U910, Prasad, Chitra; University of Western Ontario, Department of Genetics, Metabolism and Pediatrics Paton, Tara; The Hospital for Sick Children, Paterson, Andrew; The Hospital for Sick Children, Roslin, Nicole; The Hospital for Sick Children, Marshall, Christian; The Hospital for Sick Children, Desvignes, Jean-Pierre; Aix Marseille Université, Roeckel-Trevisiol, Nathalie; Aix Marseille Université, Scherer, Stephen; Hospital for Sick Children, Genetics & Genome Biology; University of Toronto, Molecular Genetics Rouleau, Guy; McGill university, Montreal Neurological institute Megarbane, Andre; Université Saint Joseph, Isaya, Grazia; Mayo Clinic, Delague, Valerie; Aix Marseille Université, Yoon, Grace; Division of Clinical and Metabolic Genetics, University of Toronto
Subject category:	Movement disorders

To search keyword list, use whole or part words followed by an *:	Ataxia < MOVEMENT DISORDERS, Genetics: movement disorders < GENETICS, Whole-exome sequencing < GENETICS, Cerebellar function < MOVEMENT DISORDERS, Gait < MOVEMENT DISORDERS

PMPCA Mutations cause Abnormal Mitochondrial Protein Processing in Patients with Non-Progressive Cerebellar Ataxia

Rebekah K. Jobling[1†], Mirna Assoum[2,3†], Oleksandr Gakh[4], Susan Blaser[5], Julian A. Raiman[1], Cyril Mignot[6], Emmanuel Roze[7,8,9,10,11], Alexandra Dürr[7,8,9,10,12], Alexis Brice[7,8,9,10,12], Nicolas Lévy[2,3,13], Chitra Prasad[14], Tara Paton[15], Andrew D. Paterson[15], Nicole M. Roslin[15], Christian R. Marshall[15], Jean-Pierre Desvignes[2,3], Nathalie Roëckel-Trevisiol[2,3], Stephen W. Scherer[15,16], Guy A. Rouleau[17], André Mégarbané[18, §], Grazia Isaya[4§], Valérie Delague[2,3§*], Grace Yoon[1, 19§*]

1) Division of Clinical and Metabolic Genetics, The Hospital for Sick Children, University of Toronto, Toronto, ON, Canada
2) Inserm, UMR_S 910, 13385, Marseille, France
3) Aix Marseille Université, GMGF, 13385, Marseille, France
4) Department of Pediatric & Adolescent Medicine and Mayo Clinic Children's Center, Mayo Clinic, Rochester, MN, USA
5) Division of Neuroradiology, The Hospital for Sick Children, University of Toronto, Toronto, Ontario, Canada
6) Département de Génétique, Unité de Génétique Clinique, APHP, Groupe Hospitalier Pitié-Salpêtrière; Centre de Référence Maladies Rares "Déficiences Intellectuelles de Causes Rares"; Groupe de Recherche Clinique UPMC Univ Paris 06; Paris, France
7) Sorbonne Université, UPMC Univ Paris 06, UM 75, ICM, F-75013 Paris, France
8) Inserm, U 1127, ICM, F-75013 Paris, France
9) Cnrs, UMR 7225, ICM, F-75013 Paris, France
10) ICM, Paris, F-75013 Paris, France
11) AP-HP, Hôpital de la Salpêtrière, Département de Neurologie, F-75013, Paris, France
12) AP-HP, Hôpital de la Salpêtrière, Département de Génétique et Cytogénétique, F-75013, Paris, France
13) Département de Génétique Médicale, Hôpital d'Enfants de la Timone, AP-HM, Marseille, France
14) Medical Genetics Program, Department of Pediatrics, London Health Sciences Centre, London, Ontario, Canada
15) The Centre for Applied Genomics and Program in Genetics and Genome Biology, The Hospital for Sick Children, Toronto, ON, Canada
16) McLaughlin Centre and Department of Molecular Genetics, University of Toronto
17) Montreal Neurological Institute and Hospital and Department of Neurology and Neurosurgery, McGill University, Montreal, QC, Canada
18) Unité de Génétique Médicale and Laboratoire Associé Inserm UMR S_910, Faculté de Médecine, Université Saint Joseph, Beirut, Lebanon
19) Division of Neurology, The Hospital for Sick Children, University of Toronto, Toronto, ON, Canada

† Joint first authors
§ These authors contributed equally to this work
* Correspondence to: Grace Yoon, Division of Clinical and Metabolic Genetics, 555 University

Avenue, Toronto, Ontario, Canada M5G 1X8. E-mail: grace.yoon@utoronto.ca
* Correspondence to: Valérie Delague, UMR_S 910, Faculté de Médecine de la Timone, 13385 Marseille cedex 05, France. E-mail: valerie.delague@univ-amu.fr

Running Title: *PMPCA* mutations in Non-progressive Cerebellar Ataxia

Abstract

Non-progressive cerebellar ataxias are a rare group of disorders which comprise approximately 10% of static infantile encephalopathies. We report the identification of mutations in *PMPCA* in 17 patients from 4 families affected with cerebellar ataxia, including the large Lebanese family previously described with autosomal recessive cerebellar ataxia and short stature of Norman type and localized to chromosome 9q34 (OMIM #213200). All patients present with non-progressive cerebellar ataxia, and the majority have intellectual disability of variable severity. *PMPCA* encodes α-MPP, the alpha subunit of mitochondrial processing peptidase, the primary enzyme responsible for the maturation of the vast majority of nuclear-encoded mitochondrial proteins, which is necessary for life at the cellular level. Analysis of lymphoblastoid cells and fibroblasts from patients homozygous for the *PMPCA* p.Ala377Thr mutation and carriers demonstrate that the mutation impacts both the level of the alpha subunit encoded by *PMPCA* and the function of mitochondrial processing peptidase. In particular, this mutation impacts the maturation process of frataxin, the protein which is depleted in Friedreich ataxia. This study represents the first time that defects in *PMPCA* and mitochondrial processing peptidase have been described in association with a disease phenotype in humans.

Keywords: Cerebellar atrophy, *PMPCA*, mitochondrial processing peptidase, ataxia, non-progressive, mitochondrial protein processing

Abbreviations: MPP = mitochondrial processing peptidase, SNP = single nucleotide polymorphism, SNV = single nucleotide variant, HGDP = The Human Genome Diversity Panel, DLD = dihydrolipoamide dehydrogenase, NFS1 = cysteine desulfurase, PRDX3 = peroxiredoxin 3, FXN = frataxin, NPCA= Non-progressive Cerebellar Ataxia

Introduction

Non-progressive cerebellar ataxias (NPCAs) manifest in infancy with abnormal gross motor development and hypotonia, followed by the appearance of ataxia (Steinlin, 1998). Dysarthria, intellectual disability and spasticity are often present (Harding, 1992). Only 7 genes/loci have been described for autosomal recessive NPCA with cerebellar atrophy to date including: Cayman type cerebellar ataxia due to mutations in *ATCAY* (OMIM #608179) (Bomar *et al.*, 2003), Spinocerebellar Ataxia 6 (SCAR6) , localized to chromosome 20q11–q13 (OMIM #608029) (Tranebjaerg *et al.*, 2003), Cerebellar Hypoplasia and Mental Retardation with or without Quadrupedal Locomotion 1 (previously Disequilibrium Syndrome, OMIM #224050) due to mutations in *VLDLR* (Boycott *et al.*, 2005), **Spinocerebellar Ataxia 14 (SCAR14) due to mutations in *STPBN2* (Lise *et al.,* 2012), a recently described family with mutations in *CWF19L1* (Burns *et al.,* 2014)**, Cerebellar Ataxia with Mental Retardation, Optic Atrophy and Skin Abnormalities (*SCAR*5) at chromosome 15q24–q26 (Delague *et al.*, 2002), due to mutations in *ZNF592* (Nicolas *et al.*, 2010), and 'Norman-type' Ataxia (SCAR2) (Mégarbané *et al.*, 1999), at chromosome 9q34–9qter (Delague *et al.*, 2001) (OMIM #213200), for which we report the identification of *PMPCA* as the causative gene. **We describe 17 patients with an NPCA phenotype, 16 with a homozygous missense mutation, p.Ala377Thr, and one with compound heterozygous mutations p.Ser96Leu and p.Gly515Arg.**

Mitochondrial dysfunction is a frequent cause of cerebellar disorders (Al-Maawali *et al.,* 2012). This dysfunction may be directly related to defects in the respiratory chain or other metabolic pathways within the mitochondria. *PMPCA* (9q34.3) encodes α -MPP, the α subunit of Mitochondrial Processing Peptidase (MPP), a heterodimeric enzyme responsible for the cleavage

of nuclear-encoded mitochondrial precursor proteins after import in the mitochondria (reviewed in Gakh *et al.,* 2002). While mitochondria contain a separate genome, the vast majority of proteins operating within the mitochondria are encoded in the nuclear genome and synthesized in the cytosol. Most nuclear-encoded mitochondrial proteins destined for the mitochondrial matrix are synthesized with an N-terminal pre-sequence required for targeting to and import into the mitochondrion. These pre-sequences usually comprise a positively charged amphipathic α-helix with hydrophobic residues on one side and hydrophilic residues at the other side of the α-helix, ranging on average from 10-60 amino acids in length (Kulawiak *et al*., 2013; Vögtle *et al*., 2009). After protein import is complete, the pre-sequence is proteolytically cleaved in one or more steps; a crucial process for normal folding and activity of the mature protein. The initial cleavage of mitochondrial matrix-targeting presequences, and in some cases subsequent cleavage, is performed by mitochondrial processing peptidase (MPP). This heterodimeric peptidase consists of an alpha subunit (α-MPP) and a beta subunit (β-MPP), both essential for enzyme activity (Hawlitschek *et al*., 1988). Deletion of the gene encoding α-MPP or β-MPP is incompatible with the viability of the unicellular organism *Saccharomyces cerevisiae* even during anaerobic growth (Pollock *et al*., 1988). In yeast cells where either subunit of MPP is depleted, the mitochondria continue to import proteins, but cleavage ceases, precursor proteins accumulate, and the affected cells eventually stop growing (Geli *et al*., 1990). Thus each of the two MPP subunits is part of a small group of components of the mitochondrial protein import machinery that are essential for life at the cellular level (reviewed in Neupert, 1997).

The β-MPP subunit is a zinc-metalloprotease containing a highly conserved zinc-binding motif located within the active site, an internal cavity between the two subunits (Taylor *et al*.,

2001). The α-MPP subunit can bind precursor proteins in the absence of β-MPP with the same efficiency as the MPP heterodimer but does not cleave the substrate (Luciano *et al*., 1997). Moreover, the α-MPP subunit undergoes a conformational change in the presence of the substrate, whereas the β-MPP subunit does not (Gakh *et al*., 2001; Janata *et al*., 2004). Together these data indicate that α-MPP is uniquely involved in substrate recognition and binding. Additional data suggest that α-MPP may achieve its function through a highly conserved, flexible glycine-rich loop which is situated at the entrance to the β-MPP active site. Alterations to the glycine-rich loop dramatically decrease or destroy the affinity for substrate and processing ability of MPP (Nagao *et al.,* 2000). A recent computational study predicted a complex, multi-step role for the glycine-rich loop in recognition and translocation of the substrate into the active site, as well as an important role in overall stability of the quaternary structure of MPP (Kučera *et al*., 2013).

Of the many mitochondrial protein precursors cleaved by MPP, one of the most well studied is human frataxin (FXN), depletion of which is known to cause Friedreich ataxia (OMIM #229300). FXN is a nuclear-encoded mitochondrial protein which undergoes cleavage by MPP after import into the mitochondria. Unlike most substrates of MPP described thus far which appear to undergo a single cleavage step from precursor to mature protein, FXN is known to undergo two cleavage reactions which require MPP (Schmucker *et al*., 2008; Cavadini *et al*., 2000). FXN enters the mitochondria as a precursor polypeptide (FXN1-210), and is sequentially cleaved by MPP to an intermediate-size form (FXN42-210) and a shorter form (FXN81-210), which are both present in cells at steady state and appear to play complementary roles in iron-sulfur cluster synthesis (Gakh *et al*., 2010; Bridwell-Rabb *et al.* 2014).

We report the identification of *PMPCA* as the causative gene for a Non-progressive Autosomal Recessive Cerebellar Ataxia syndrome (SCAR2), previously mapped to chromosome 9q34 (Delague *et al.*, 2001) in17 patients from four families. Functional analyses confirm a significant impact of mutations in *PMPCA* on MPP function. To our knowledge, this is the first report of MPP dysfunction in humans, and further highlights the importance of mitochondrial function in human cerebellar disorders.

Materials and Methods

Subjects

Seventeen patients from four families have been included in this study (Fig. 1) Families 1-3 are Christian Lebanese Maronite families from North-East Lebanon (Békaa Valley/Mount Lebanon). **Clinical characteristics of our patients are summarized in Table 1.** After informed consent was obtained from all individuals and parents of children included in this study, EDTA blood samples were collected, and genomic DNA was extracted from lymphocytes with the use of standard methods. All protocols performed in this study complied with the ethics guidelines of the institutions involved.

Family 1 (F1)

Family 1 is a large consanguineous Christian Lebanese Maronite originating from a village from North-East Lebanon. Thirty two members from this large family had been previously described as affected with hereditary non progressive cerebellar ataxia and short stature (Mégarbané *et al.*, 1999). Briefly, the 12 affected members presented with a delay in psychomotor development and ataxic gait which varied from mild to severe. Dysarthria, increased deep tendon reflexes, hypotonia and/or spasticity, slightly diminished muscle strength, flat feet, short stature ranging

from <10th to <3rd percentile, moderate to severe intellectual deficiency, and visuo-spatial defects were also observed. MRI performed on members of this family revealed pronounced cerebellar vermis and bilateral hemisphere atrophy, a dilated fourth ventricle, and a large cisterna magna. Because of similar clinical features, we described this disease as Nonprogressive Cerebellar Ataxia of Norman type, also referred to as Spinocerebellar Ataxia, Autosomal Recessive 2 (SCAR2) (OMIM 213200).

Family 2 (F2)

Patient F2-II.1, a male, was the first child of a G3P0SA2 mother, following an uncomplicated pregnancy. Family history was non-contributory, and the parents, who were both born and raised in Canada, were unaware of any consanguinity, though their ancestors are Christian Lebanese Maronites from the same village in Lebanon. Gross motor milestones were initially normal; the patient stood with support at 10 months of age, and was cruising at 11 months. However, between the ages of 11 and 15 months there was a gradual loss of these skills. His parents noted unsteadiness at 18 months of age, and on examination at 2 years he had truncal and gait ataxia, generalized hypotonia and intention tremor. After this there was stabilization and slow improvement. At the age of 9 years, he could walk short distances unassisted, but required a walker for longer distances. Fine motor skills were also delayed; at 9 years he had difficulty writing and used a computer in class. Initial expressive and receptive language development was normal, but dysarthria was noted between the ages 2 and 4 years. He was performing at grade level in school. On examination at 9 years of age he had saccadic smooth pursuit, gait ataxia, dysmetria, dysdiadochokinesis and impaired fast finger movements. MRI studies revealed atrophy of the cerebellar vermis and hemispheres (Fig. 2a, 2b). Sanger sequencing of the coding regions of *FXN*, *POLG*, *APTX* and *PLA2G6*, as well as a microarray did not reveal variants

which were bioinformatically predicted to be damaging, and routine metabolic studies were normal. **Electromyogram and nerve conduction studies were normal.** Muscle biopsy at the age of 4 years revealed mild, nonspecific myopathic changes, including rare atrophic fibers and fibers with central nuclei. **Electron microscopy studies of the muscle were normal.** Respiratory chain analysis on muscle tissue revealed decreased activity of complexes I and III and II and III. Further studies on fibroblasts revealed mildly decreased activity of complex I and III, and isolated complex III activity in the low-normal range. Coenzyme Q10 analysis of muscle was normal.

Patient F2-II.2, the younger brother of patient F2-II.1 was born following a normal pregnancy, with delivery at 37 weeks due to fetal bradycardia and a nuchal cord. Delivery was vaginal with forceps. Development was normal until the age of 12 months, at which time he was standing with support, cruising and had 7 words. Over the next 5 months he developed limb and gait ataxia. At 15 months he lost his previously normal pincer grasp and used a palmar grasp. Examination at 2 years and 6 months revealed significant truncal and gait ataxia, as well as tremor. Since then there has been stabilization and slow improvement. At the age of 7 years he continued to have very little speech. Neurocognitive assessment revealed intellectual disability. Serial MRI revealed atrophy of the cerebellar vermis and hemispheres identical to that of his brother (Fig 2c, 2d).

Family 3 (F3)

Family 3 is a consanguineous Christian Maronite Lebanese family originating from the Békaa valley.

Patient F3-V.2, a female born in Lebanon, was born at term after an uneventful pregnancy. Truncal hypotonia was noted since birth and gradually improved with time. She had global

developmental delay; her first words were at 7 years and she walked unaided at 9 years. She attended a special school in Lebanon and was unable to learn to read. Neurological examination at age 33 revealed moderate cerebellar dysfunction; gait ataxia, dysmetric saccades and gaze-evoked nystagmus, dysarthria and dysmetria. **(Supplemental video).** She had no pyramidal, or extrapyramidal manifestations, and no signs suggesting peripheral neuropathy. She was treated with fluoxetine for depression. Routine metabolic testing in blood and cerebrospinal fluid, urine purines and pyrimidines, lysosomal enzyme activities in leukocytes, pristanic and phytanic acids and karyotype were normal. Ophthalmologic examination revealed myopia and was otherwise normal. At age 40 years, her height was 156 cm, which was consistent with her family, and her occipitofrontal circumference was normal at 54 cm. Neuropsychological evaluation revealed intellectual deficiency (verbal IQ 47, performance IQ 49). Brain MRI demonstrated cerebellar atrophy with vermian predominance (Fig. 2e). **Neurological examination revealed no change from her previous evaluation at 33 years. (Supplemental video)**

Patient F3-V.5 was the younger sister of patient F3-V.2. Prenatal and neonatal history was normal. She had always been ataxic and learned to walk unaided at age 9 years. She spoke at 4 years and attended a special school in Lebanon where she learned to read with difficulties. At first examination at the age of 12 years she had cerebellar dysfunction, and brain MRI revealed cerebellar atrophy. When re-examined at 22 years, she had mild ataxic gait, mild dysarthria, dysmetria of the upper and lower limbs and gaze-evoked nystagmus. Her occipitofrontal circumference was normal. There were no pyramidal or extrapyramidal signs and no peripheral neuropathy. Her intellectual development was that of a 10-12 year-old child although she was not formally tested.

Family 4 (F4)

Patient F4-II.1, a male patient, was born to a non-consanguineous French couple with no familial history of ataxia. His sister was also affected but was never examined. She had depressed mood since the age of 14 and died at 29 years, possibly of suicide. He walked after the age of 2 years and was diagnosed with ataxia because of frequent falls. He is now 58 years, and was last examined at the age of 43 years. When examined at 43 years, he had mild gait ataxia, dysmetria of the upper limbs, gaze-evoked nystagmus and dysarthria. He had completed education at the post-secondary level and his neurological status was stable over time. Brain MRI demonstrated cerebellar atrophy with vermian predominance.

Results

Mutation Identification and Modelling

Homozygosity mapping performed in family 1 previously allowed the assignment of the disease locus to a 12.1-cM interval on chromosome 9q34-qter between markers D9S67 and D9S312 (Delague *et al.*, 2001). Since the first description of the locus, completion of the genomic sequence at 9q34 led to a reassignment of some microsatellite markers, allowing refining of the linkage region to a 2.85 Mb region between D9S67 and the 9q telomere. In this region, we sequenced 17 candidate genes by standard Sanger sequencing: *BARHL1*, *INPP5E*, *NOTCH1*, *NPDC*, *TRAF2*, *TUBB2C*, *ZYMND19*, *SLC34A3*, *KCNT1*, *LCN1*, *TMEM141*, *PHPT1*, *PAEP*, *QSOX2* and *PMPCA.* A homozygous c.1129G>A transition (p.Ala377Thr) in *PMPCA* (NM_015160) exon 10 was identified in all patients and found to segregate with the disease phenotype (Fig. 3A and data not shown).

In parallel, exome sequencing was performed in patient F1-VI.2. After variant annotation and filtering, two rare candidate variants were located within 2.95 Mb linkage region distal to D9S67

identified previously: the c.1129G>A transition (p.Ala377Thr) already identified in *PMPCA* (NM_015160) by Sanger sequencing of candidate genes, and a c.2453C>T transition (p.Ala818Val) in *CAMSAP1* (NM_015447).

Exome sequencing in patient F2-II.1 was undertaken. Homozygosity mapping performed previously in family 2 allowed the identification of 7 candidate homozygous by descent regions. Analysis of the homozygous variants, within the linked regions, revealed only one variant present at less than 1% frequency in the public population databases: the same missense variant in *PMPCA*, NM_015160.1:c.1129G>A p.Ala377Thr identified in family 1, which after Sanger sequencing, was shown to segregate in the pedigree. The variant in *CAMSAP1* was absent in this family.

The *PMPCA* p.Ala377Thr variant was absent in 916 Lebanese control chromosomes, and was not present in any of the public single nucleotide polymorphism or variant databases.

RT-PCR on total RNA extracted from lymphoblastoid cell lines from patients F1-VI.8, F1-VI.15, and F1-VI.22 from family 1, using primers located in *PMPCA* exons 8 and 12 did not show evidence any abnormal transcript, thus ruling out a possible splicing defect associated with this specific variant. (Fig. 3A and data not shown)

We screened the *PMPCA* coding sequence in a cohort of 39 French patients with NPCA and identified two additional patients with variants in *PMPCA*: patient F3-V.2, who was homozygous for the same missense p.Ala377Thr variant and patient F4-II.1, who was compound heterozygous for two missense variants: c.287C>T (p.Ser96Leu) and c.1543G>A (p.Gly515Arg) (Fig. 3A and data not shown). Patient F3-V.2 proved to be of Lebanese origin and her sister, patient F3-V.5, was also homozygous for the same variant. The c.287C>T

(p.Ser96Leu) and c.1543G>A (p.Gly515Arg) variants were absent in 372 French chromosomes and not present in any public single nucleotide polymorphism or variant databases.

All three variants affect amino acid residues highly conserved in α-MPP sequences across vertebrates, invertebrates and most metazoans. (Fig. 3B). They are predicted to be pathogenic by multiple prediction software programs including SIFT, Provean, Polyphen-2, MutationTaster, Provean, Panther and UMD predictor.

The alanine residue at position 377 (human numbering) lies only 20 residues downstream from the glycine-rich region (Fig. 3B). Homology modeling suggests that Ala377 is in close proximity to the glycine-rich loop (Fig. 3C). The bulkier side chain of threonine at position 377 in our patients' α-MPP may interfere with the flexibility of the glycine-rich loop, and therefore the ability of MPP to bind substrates in a stable fashion. The two other missense variations Ser96Leu and Gly515Arg are located within two conserved regions of the peptidase (Fig. 3B).

Founder effect

Genotyping of 6 STRs and 8 SNPs was performed for the 16 Lebanese patients from families F1, F2 and F3. (Supplementary Table S1) Reconstruction of the haplotypes in the three families demonstrated that patients from families F2 and F3 are homozygous by descent for a ~4 Mb region distal to the D9S1818 STR marker, whereas this region was smaller in family F1 (2.83 Mb, distal to the rs2004074 SNP marker). This is due to the large size of family F1 and the numerous recombination events which occurred during meiosis since the mutation first occurred in the common ancestor.

PMPCA expression

Semi-quantitative RT-PCR in human adult and fetal tissues showed that *PMPCA* is expressed in all tissues with relatively higher levels of expression in adult brain, cerebellum, and cerebellar vermis (Fig. 4).

Quantitative Studies of MPP Subunit Levels

Western blot analysis of immortalized lymphoblastoid cell lines from family 2 revealed markedly decreased levels of α-MPP in the two patients and intermediate levels in both carrier parents compared to controls (Fig. 5A). Densitometry measurements revealed that α-MPP levels were 33% and 34% in patient F2 II.1 and F2 II.2, and 65% and 57% in the two carrier parents relative to α-MPP levels in the controls (Fig. 5A-B). The intermediate α-MPP level in the carrier parents supported that it was the Ala377Thr mutation which was responsible for the decreased α-MPP. Levels of α-MPP were also quantified in lymphoblastoid cells and fibroblasts from patients from family 1 and controls. The results from two independent experiments showed a mean decrease of 25%, 50% and 44% of α-MPP levels in lymphoblastoid cells from patients F1-VI.8, F1-VI.15, F1-VI.22, respectively, and a 54% decrease in fibroblasts from patient F1-VI.22 (data not shown).

The levels of β-MPP were examined in family 2 by western blotting with anti-β-MPP polyclonal antibody, and densitometry and found to be similar between the two patients and the carriers or controls (Supplementary Fig. S1).

MPP Function

To assess potential functional effects of the Ala377Thr mutation, we analyzed the steady-state levels of the mature forms of four nuclear-encoded mitochondrial matrix proteins: dihydrolipoamide dehydrogenase (DLD), cysteine desulfurase (NFS1), peroxiredoxin 3 (PRDX3) and FXN (Fig. 5A), in patients and carriers from family 2, and controls. The levels of

DLD, NFS1 and PRDX3 appeared similar in both carrier and patient lymphoblasts compared to controls, suggesting that the mutation does not alter the ability of MPP to process these particular precursor proteins, at least not to an extent appreciable by western blotting. However, the cleavage of FXN appeared altered in carriers and patients. The carrier parents' lymphoblast cell extracts demonstrated a small accumulation of the intermediate isoform FXN42-210, but no noticeable change in FXN81-210 or other FXN isoforms compared to controls (Figs. 5A and 6). Moreover, the affected patients demonstrated several abnormalities of FXN processing including accumulation of FXN42-210 (~300% of normal levels), reduction of FXN81-210 (~50% of normal levels) (Figs. 5A and 6), and accumulation of the FXN56-210 isoform, which was not detected in the controls and was detected as a faint band in one of the carrier parents (Fig. 5A). The total levels of all FXN isoforms in the patients were ~150% of control levels (Fig. 6).

As a measure of REDOX balance in the mitochondria, the ratio of oxidized/reduced PRDX3 was assessed via western blotting and densitometry (Fig. 5A) (Kumar *et al.*, 2009). The ratio in the patients was increased over both the control and carrier levels while they were similar between carriers and controls (Supplementary Fig. S2).

Subcellular localization

We carried out immunofluorescent labeling of α-MPP and CoxIV, one of the nucleus-encoded subunit of cytochrome c oxidase, the terminal enzyme complex of the mitochondrial electron transport chain located at the inner mitochondrial membrane, in fibroblasts from patient F1-VI.22 and one control. Co-localization of α-MPP and CoxIV and the morphology of the mitochondrial reticulum appeared similar between patient and control cells (Fig. 7).

Discussion

The α-MPP protein, encoded by *PMPCA*, is necessary for cell survival. Without functional α-MPP, nucleus-encoded mitochondrial precursor proteins accumulate inside mitochondria and the MPP-deficient cells stop growing (Geli *et al*., 1990). The requirement of MPP, and therefore α-MPP, for cell survival can be attributed to the large number of mitochondrial proteins that require precursor cleavage to attain their mature and functional form. Accumulation of a variety of non-functional or poorly functional mitochondrial proteins disrupts mitochondrial function and causes loss of cell viability even in the facultative anaerobe *S. cerevisiae* (Pollock *et al*., 1988; Geli *et al*., 1990). This vital biological function renders it unlikely that mutations that cause complete loss of α-MPP or widespread disruption of MPP cleavage reactions would be common in humans. However, our patients demonstrate that partial disruption in MPP function can be compatible with life although with severe phenotypic consequences. Indeed, the c.1129G>A (p.Ala377Thr) mutation decreased the level of α-MPP, yet the residual level of functioning MPP was sufficient to maintain mitochondrial biogenesis and overall viability. The presence of this mutation does perturb the function of MPP with respect to the cleavage of FXN. The initial cleavage step from precursor FXN1-210 to intermediate FXN42-210 appears to be intact as we did not detect any accumulation of FXN1-210. However, the subsequent cleavage to FXN81-210 is impaired, leading to a three-fold accumulation of FXN42-210. The generation of excess FXN56-210 is also seen in the patient cells. This isoform is detected at very low levels under normal conditions (Gakh *et al*., 2010), but has been demonstrated to accumulate in the context of disruption of either the initial or second cleavage steps, or with a 20-fold over-expression of FXN1-210 (Schmucker *et al*., 2008).

The second cleavage step occurs at a slower rate than the first, and is rate-limiting for the formation of mature protein (Cavadini *et al*., 2000; Schmucker *et al*., 2008). We proposed that the structure of the presequence of the human frataxin precursor is responsible for the low rate at which FXN42-210 is processed to mature form and/or that the first cleavage results in a conformational change that affects the ability of MPP to carry out the second cleavage (Cavadini *et al*., 2000). If the Ala377Thr mutation impacts the flexibility of the glycine-rich loop of α-MPP, which is important for recognition and translocation of the substrate into the peptidase active site (Kučera *et al*., 2013), a cleavage reaction that is particularly dependent on structural determinants would be more likely to be affected. **The Ser96Leu and Gly515Arg mutations may affect the folding of other conserved regions of the peptidase, and perhaps the stability of the entire alpha subunit given the longer side chains of Leu and Arg; however this remains to be verified in future studies.**

The non-progressive clinical phenotype of our patients differs from the progressive course with death at a young age typically seen in patients with Friedreich ataxia, which results from global depletion of all frataxin isoforms. In this respect, it is notable that while the levels of FXN81-210 in our patients were as low as those in Friedreich ataxia patients, the levels of FXN42-210 were much higher in our patients compared to Friedreich ataxia patients and, to a lesser extent, carriers and controls. FXN42-210 and FXN81-210 have been proposed to have complementary functions and were consistently detected in normal lymphoblastoid cells and cerebellum with a FXN81-210:FXN42-210 ratio of approximately 2:1 (Gakh *et al*., 2010). Therefore, it is possible that abnormal FXN processing contribute to disease pathophysiology in our patients by altering the FXN81-210/FXN42-210 ratio.

Our analysis also suggests the Ala377Thr mutation leads to more general abnormalities of mitochondrial function. The increased ratio of oxidized to reduced PRDX3 is an indication of increased hydrogen peroxide in mitochondria (Kumar *et al*., 2009), which may be due to reduced electron flux through the respiratory chain, leading to increased reactive oxygen species formation. It is possible that the mild disturbance of oxidative phosphorylation in muscle tissue from F2-II.1 may be secondary consequence of one or more defects in the processing of nucleus-encoded respiratory chain proteins.

Mitochondrial dysfunction is an established cause of cerebellar atrophy. It is unlikely that the pathogenesis of cerebellar atrophy in these patients is solely related to dysfunction of FXN, since our patients do not display the typical clinical features or MRI findings of Friedreich ataxia. **(Supplementary Fig. S3)** Moreover, the vast majority of precursor cleavage reactions performed by MPP have not been evaluated in our patients and it is possible that other cleavage reactions are also affected. Nevertheless, the finding of both decreased levels of α-MPP and disruption of FXN processing in association with mutations in *PMPCA* in multiple patients from different families with almost identical phenotypes argues strongly for a role for MPP dysfunction in this disease process.

We present 17 patients from 4 families with cerebellar atrophy and non-progressive cerebellar ataxia (NPCA). **All patients presented with hypotonia and gross motor delay, with or without initial worsening of their symptoms which then stabilized and did not progress even after decades, and serial brain imaging revealed stable cerebellar atrophy.** We

identified a homozygous missense c.1129G>A (p.Ala377Thr) mutation in *PMPCA* (NM_015160) in 16 Lebanese patients from 3 families and two compound heterozygous missense variations in one French patient: c.287C>T (p.Ser96Leu) and c.1543G>A (p.Gly515Arg), in *PMPCA* exons 3 and 13 respectively. All mutations segregated with the disease phenotype, were not found in control chromosomes, nor in any of the public single nucleotide polymorphism or variant databases. We describe a founder effect for the c.1129G>A (p.Ala377Thr) mutation, as patients from 3 *a priori* non-related Lebanese families share a common 2.3 Mb homozygous region at 9q34.3 surrounding the *PMPCA* gene. Functional studies confirmed the deleterious effect of *PMPCA* mutations on MPP function, which definitely implicates *PMPCA* as the causal gene in this rare form of NPCA. This is the first time that the MPP enzyme, vital to life at the cellular level, has been associated with a clinical phenotype in humans. Disruption of mitochondrial protein precursor cleavage represents a new avenue for investigation of the pathogenesis of non-progressive cerebellar ataxia.

Acknowledgments

We would like to thank the patients and families for their participation in this study. We would also like to thank Dr. Frantisek Kalousek (Department of Genetics, Yale University, New Haven, CT, USA) and Dr. Jiri Janata (Institute of Microbiology, Academy of Sciences of the Czech Republic, Prague, Czech Republic) for providing the anti-MPP polyclonal antibodies, and Dr. Tibor Bedekovics (Mayo Clinic, Rochester, MN, USA) for help in the characterization of the antibodies. We are grateful to all the members of the Medical Genetics Unit from Saint-Joseph University, in particular Nabiha Salem and Eliane Chouery, and to Dr Farid Stephan from Hotel-

Dieu de France in Beirut. We would like to thank Dr Marc Bartoli for his advice on this project. We are also grateful to Rania Nakad and Chawki Harfouche for their technical assistance.

Funding

This work was supported in part by a grant from the National Institutes of Health, National Institute on Aging, AG15709-18 (to GI). Financial support was also obtained from The Centre for Applied Genomics and the University of Toronto McLaughlin Centre, Saint-Joseph University (USJ) and the Institut National de la Santé et de la Recherche Médicale (Inserm).This study was partly sponsored by the French Association against Myopathies "Association Française contre les Myopathies" (AFM), the "Agence Universitaire de la Francophonie" (AUF) and the European Union's Seventh Framework Programme for research, technological development and demonstration under grant agreement n°294983 (LEB'IN project:Lebanon-Europe "on boarding" to innovate and enhance research links in health).

Mirna Assoum was supported by a grant from the the Institut National de la Santé et de la Recherche Médicale (Inserm) and by the European Union (LEB'IN project: grant agreement n°294983).

Conflict of Interest

Mayo Clinic has a financial interest associated with technology used in the author's research, which has been licensed to a commercial entity. Mayo Clinic, but not the authors, has received royalties of less than the federal threshold for significant financial interest.

Supplementary Material

Supplementary Materials and Methods, Figures, and Tables, are provided as separate PDF files. Supplementary Videos are available online on the journal website.

References

Al-Maawali A, Blaser S, Yoon G. Diagnostic approach to childhood-onset cerebellar atrophy: a 10-year retrospective study of 300 patients. J. Child Neurol 2012; *27*: 1121–1132.

Bomar JM, Benke PJ, Slattery EL, Puttagunta R, Taylor LP, Seong E, et al. Mutations in a novel gene encoding a CRAL-TRIO domain cause human Cayman ataxia and ataxia/dystonia in the jittery mouse. Nat Genet. 2003;35(3):264-9.

Boycott KM, Flavelle S, Bureau A, Glass HC, Fujiwara TM, Wirrell E, et al. Homozygous deletion of the very low density lipoprotein receptor gene causes autosomal recessive cerebellar hypoplasia with cerebral gyral simplification. Am J Hum Genet. 2005;77(3):477-83.

Bridwell-Rabb J, Fox NG, Tsai CL, Winn AM, Barondeau DP. Human frataxin activates Fe-S cluster biosynthesis by facilitating sulfur transfer chemistry. Biochemistry. 2014 Aug 5;53(30):4904-13

Burns R, Majczenko K, Xu J, Peng W, Yapici Z, Dowling JJ et al. Homozygous splice mutation in CWF19L1 in a Turkish family with recessive ataxia syndrome. Neurology. 2014; 83:1–8.

Cavadini P, Adamec J, Taroni F, Gakh O, Isaya G. Two-step processing of human frataxin by mitochondrial processing peptidase. Precursor and intermediate forms are cleaved at different rates. J. Biol. Chem. 2000; *275*:41469–41475.

Choi Y, Sims GE, Murphy S, Miller JR, Chan AP. Predicting the functional effect of amino acid substitutions and indels. PloS one. 2012;7(10):e46688.

Delague V, Bareil C, Bouvagnet P, Salem N, Chouery E, Loiselet J, et al. A non-progressive autosomal recessive ataxia maps to chromosome 9q34-9qter in a large consanguineous Lebanese family. Ann Neurol. 2001;50:250-3.

Delague V, Bareil C, Bouvagnet P, Salem N, Chouery E, Loiselet J, et al. A new autosomal recessive non-progressive congenital cerebellar ataxia, associated with optic atrophy and mental retardation, maps to chromosome 15q24-q26 in a large consanguineous Lebanese Druze family. Neurogenetics. 2002;4:23-7.

Gakh O, Obsil T, Adamec J, Spizek J, Amler E, Janata J, et al. Substrate binding changes conformation of the alpha-, but not the beta-subunit of mitochondrial processing peptidase. Arch Biochem. Biophys 2001; *385*: 392–396.

Gakh O, Cavadini P, Isaya G. Mitochondrial processing peptidases. Biochim Biophys Acta 2002; *1592*: 63–77.

Gakh O, Bedekovics T, Duncan SF, Smith DY, Berkholz DS, Isaya G. Normal and Friedreich ataxia cells express different isoforms of frataxin with complementary roles in iron-sulfur cluster assembly. J Biol Chem 2010; *285*: 38486–38501.

Geli V, Yang MJ, Suda K, Lustig A, Schatz G. The MAS-encoded processing protease of yeast mitochondria. Overproduction and characterization of its two nonidentical subunits. J Biol Chem 1990; *265*; 19216–19222.

Harding A. Hereditary ataxias and related disorders. In: Asbury, McKhann, McDonald, editors. Diseases of the nervous system Clinical neurobiology. 2nd ed. Philadelphia: WB Saunders Company; 1992. p. 1169-78.

Hawlitschek G, Schneider H, Schmidt B, Tropschug M, Hartl FU, Neupert W. Mitochondrial protein import: identification of processing peptidase and of PEP, a processing enhancing protein. Cell 1988; *53*: 795–806.

Janata J, Holá K, Kubala M, Gakh O, Parkhomenko N, Matusková A, et al. Substrate evokes translocation of both domains in the mitochondrial processing peptidase alpha-subunit during which the C-terminus acts as a stabilizing element. Biochem Biophys Res Commun 2004; *316*: 211–217.

Kučera T, Otyepka M, Matušková A, Samad A, Kutejová E, Janata J. A computational study of the glycine-rich loop of mitochondrial processing peptidase. PloS One 2013; *8*: e74518.

Kulawiak B, Höpker J, Gebert M, Guiard B, Wiedemann N, Gebert N. The mitochondrial protein import machinery has multiple connections to the respiratory chain. Biochim Biophys Acta 2013 *1827*, 612–626.

Kumar P, Henikoff S, Ng PC. Predicting the effects of coding non-synonymous variants on protein function using the SIFT algorithm. Nat Protoc 2009; *4*: 1073–1081.

Kumar V, Kitaeff N, Hampton MB, Cannel MB, Winterbourn CC. Reversible oxidation of mitochodrial peroxiredoxin 3 in mouse heart subjected to ischemia and reperfusion. FEBS Lett 2009; 583:997-1000.

Lise S, Clarkson Y, Perkins E, Kwasniewska A, Sadighi Akha E, Schnekenberg RP. Recessive mutations in SPTBN2 implicate β-III spectrin in both cognitive and motor development. PLoS Genet. 2012;8(12):e1003074.

Luciano P, Geoffroy S, Brandt A, Hernandez JF, Géli V. Functional cooperation of the mitochondrial processing peptidase subunits. J Mol Biol 1997; *272*: 213–225.

Mégarbané A, Delague V, Salem N, Loiselet J. Autosomal recessive congenital cerebellar hypoplasia and short stature in a large inbred family. Am J Med Genet. 1999;87(1):88-90.

Nagao Y, Kitada S, Kojima K, Toh H, Kuhara S, Ogishima T, et al. Glycine-rich region of mitochondrial processing peptidase alpha-subunit is essential for binding and cleavage of the precursor proteins. J Biol Chem 2000; *275*: 34552–34556.

Neupert W. Protein import into mitochondria. Annu Rev Biochem 1997; 66: 863-917.

Nicolas E, Poitelon Y, Chouery E, Salem N, Levy N, Megarbane A, et al. CAMOS, a nonprogressive, autosomal recessive, congenital cerebellar ataxia, is caused by a mutant zinc-finger protein, ZNF592. Eur J Hum Genet. 2010;18(10):1107-13.

Pollock RA, Hartl FU, Cheng MY, Ostermann J, Horwich A, Neupert W. The processing peptidase of yeast mitochondria: the two co-operating components MPP and PEP are structurally related. EMBO J 1988; 7: 3493-500.

Schmucker S, Argentini M, Carelle-Calmels N, Martelli A, Puccio H. The in vivo mitochondrial two-step maturation of human frataxin. Hum Mol Genet 2008; *17*: 3521–3531.

Steinlin M. Non-progressive congenital ataxias. Brain Dev. 1998;20(4):199-208.

Taylor AB, Smith BS, Kitada S, Kojima K, Miyaura H, Otwinowski Z, et al. Crystal structures of mitochondrial processing peptidase reveal the mode for specific cleavage of import signal sequences. Structure 2001; *9*: 615–625.

Tranebjaerg L, Teslovich TM, Jones M, Barmada MM, Fagerheim T, Dahl A, et al. Genome-wide homozygosity mapping localizes a gene for autosomal recessive non-progressive infantile ataxia to 20q11-q13. Hum Genet. 2003;113(3):293-5.

Vögtle, FN, Wortelkamp S, Zahedi RP, Becker D, Leidhold C, Gevaert K, et al. Global analysis of the mitochondrial N-proteome identifies a processing peptidase critical for protein stability. Cell 2009; *139*: 428–439.

Figure Legends

Figure 1. Pedigrees from all four families. Affected individuals are shaded in black.

Figure 2. Sagittal T1 weighted image (a) demonstrates moderately severe vermian atrophy in patient F2-II.1 at 21 months of age. Axial FLAIR (a1) and T2 (a2) images obtained at the same time demonstrate atrophy and abnormal signal of the cortex of the vermis and cerebellar hemispheres. Similar findings are present on subsequent sagittal T1 (b), axial FLAIR (b1) and coronal T1 weighted (b2) MRI images of the same child at 6 years 5 months of age. Sagittal T1 weighted image (c) demonstrates moderately severe vermian atrophy in his sibling, patient F2-II.2 at 15 months of age. Axial (c1) and coronal T2 weighted images (c2) obtained at the same time demonstrate atrophy and increased signal of the cortex of the vermis and cerebellar hemispheres. Similar findings are present on subsequent sagittal T1 (d), axial FLAIR (d1) and coronal T1 (d2) weighted images of the same child at 4 years 3 months of age. Finally, moderately severe vermian atrophy and abnormal signal of the cortex of vermis and cerebellar hemispheres is shown on sagittal T1 (e), Axial FLAIR (e2) and coronal T1 (e2) weighted MRI in patient F3-V.2 at 40 years of age. Supratentorial structures (not shown) were normal in signal and appearance in all at all ages. Diffusion weighted imaging for patients F2-II.1 and patient F2-II.2 showed no diffusion restriction and short echo supratentorial MRS was age appropriate without demonstrable lactate. MRS of the cerebellum was not performed.

Figure 3. A. Chromatograms showing the 3 mutations identified in *PMPCA* (NM_015160): the c.1129G>A (p.Ala377Thr) in PMPCA exon 10, the c.287C>T (p.Ser96Leu) in exon 3, and the c.1543G>A (p.Gly515Arg) in exon 13. The agarose gel shows a transcript of normal size in the lymphoblastoid cell lines from patients F1-VI.15, F1-VI.16, F1-VI.8 homozygous for the p.Ala377Thr mutation. **B.** Amino acid sequences of α-MPP from the indicated species were

aligned using the program CLUSTAL 2.0.12 on the JustBio.com online tools resource. Shown are the protein regions comprising the three mutations under investigation. The glycine-rich loop is highlighted in cyan. Alanine 377, Serine 96 and Glycine 515 (human numbering) are highlighted in red. Each of these aminoacid residues is highly conserved across mammals. **C.** A model of the structure of the human MPP heterodimer was generated by homology modeling using the program iTASSER (Supplementary Table S2). β-MPP is shown in beige with the active site residues as green sticks and the catalytic Zn^{2+} ion in gray. α-MPP is shown in pink with the glycine-rich loop in cyan and Alanine 377, Serine 96, and Glycine 515 are shown as green sticks.

Figure 4. Semiquantitative expression of *PMPCA* in different human adult (A) and fetal (B) tissues. β-actin was used for normalization.

Figure 5. A. Cell extracts from the indicated subjects were prepared from exponentially growing lymphoblastoid cell cultures and each sample (30 μg of total protein) was analyzed by 15% SDS/PAGE and western blotting with specific antibodies as described in Supplementary Materials and Methods. Blots were cropped to enable direct comparison of several different mitochondrial proteins in one figure. Full length blots are provided in Supplementary Fig. S4 A-C. **B**. Densitometry measurements of α-MPP protein bands were collected from the subjects analyzed in A. as described in Supplementary Materials and Methods. The total number of α-MPP protein bands analyzed was ≥6 for each carrier and each patient, and ≥3 for each of the controls. Each data point shows the mean of the technical replicates for each subject in the group.

Figure 6. Densitometry measurements of FXN 42-210 and FXN 81-210 protein bands were collected from the same subjects analyzed in Fig. 5 and densitometry was performed as described in Supplementary Materials and Methods. Two FXN42-210 or FXN81-210 protein

bands were analyzed for each control, FRDA patient, MPP carrier and MPP patient. Each data point shows the mean of the technical replicates for each subject in the group.

Figure 7. Immunolabeling of α-MPP and CoxIV in fibroblasts from patient VI.22 from family 1 and one control. Mitochondria were labeled using a mouse monoclonal antibody against CoxIV (cytochrome oxidase IV), located at the inner mitochondrial membrane (green signal), and α-MPP was detected using a rabbit polyclonal antibody (Novus Biologicals-NBP89126) against human α-MPP (red signal, see details in Material &Methods). Nuclei are stained with DAPI (Blue). No abnormal localization or accumulation of α-MPP was found in the 108 patients' fibroblasts as compared to 68 control cells from 3 independent experiments.

Table 1. Clinical characteristics of 17 patients with biallelic mutations in *PMPCA*.

Patient	Age (yr) at Most Recent Assessment	Intellectual Disability	Age (yr) at Language Acquisition	Age (yr) at Independent Walking	Dysarthria	Deep Tendon Reflexes	Gait Ataxia	Dysmetria	Gaze-evoked Nystagmus
F1-VI.2	25	+	5	10	+	Absent	+	+	+
F1-VI.4	22	+	4-5	9	+	Brisk	+	+	+
F1-VI.8	32	+	3	10	+	Brisk	+	+	+
F1-VI.9	33	+	4	11	+	Brisk	+	+	+
F1-VI.10	23	+	4	10	+	Brisk	+	+	+
F1-VI.15	44	+	5	12	+	Brisk	+	+	+
F1-VI.16	42	+	4	9	+	Brisk	+	+	+
F1-VI.17	40	+	5	12	+	Brisk	+	+	+
F1-VI.18	37	+	3	11	+	Brisk	+	+	+
F1-VI.21	28	+	4	11	+	Brisk	+	+	+
F1-VI.22	27	+	5	9	+	Brisk	+	+	+
F1-VI.24	46	+	4	13	+	Arms Absent/ Legs Brisk	+	+	+
F2-II.1	9	-	1	3	+	Normal	+	+	+
F2-II.2	7	+	1*	N/A**	+***	Normal	+	+	+
F3-V.2	33	+	7	9	+	Normal	+	+	+
F3-V.5	22	+	4	9	+	Normal	+	+	+
F4-II.1	43	-	U	After 2 years	+	U	+	+	+

N/A: Not Applicable, U: Unknown, *Loss of words after 1 year, ** Independent walking not yet achieved, ***Minimal language use

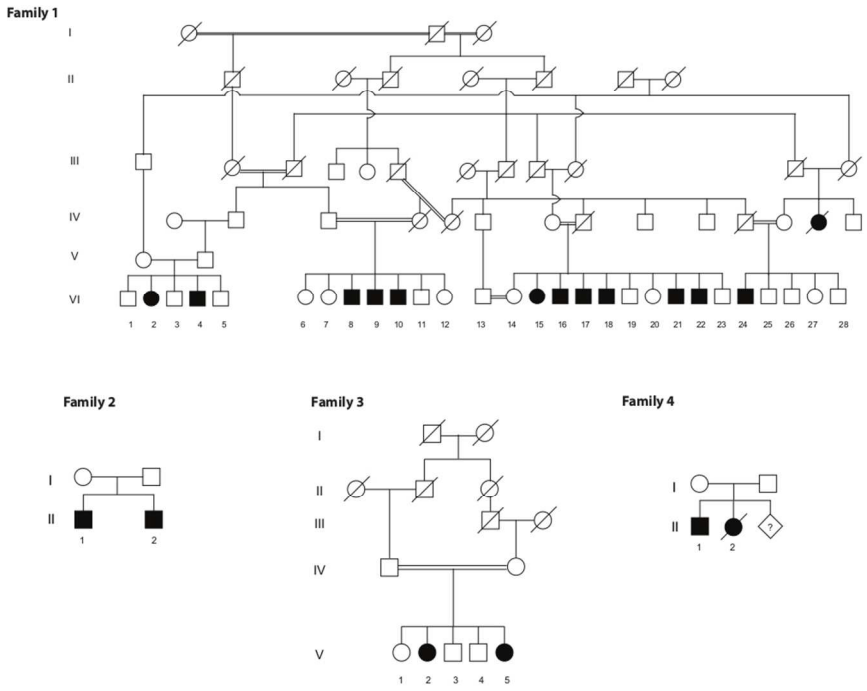

296x209mm (100 x 100 DPI)

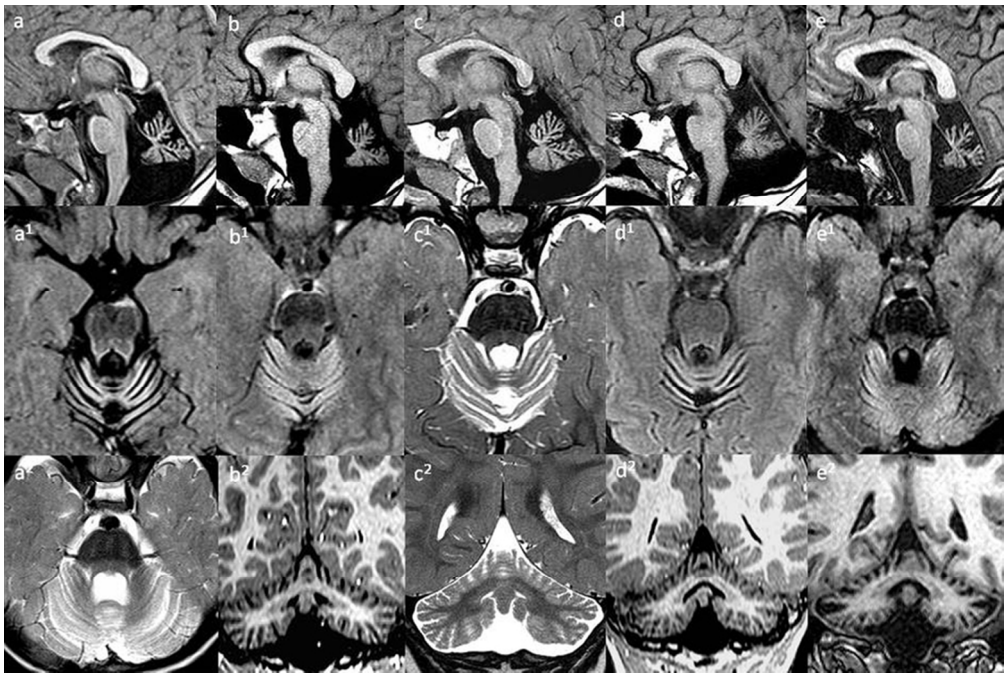

84x56mm (300 x 300 DPI)

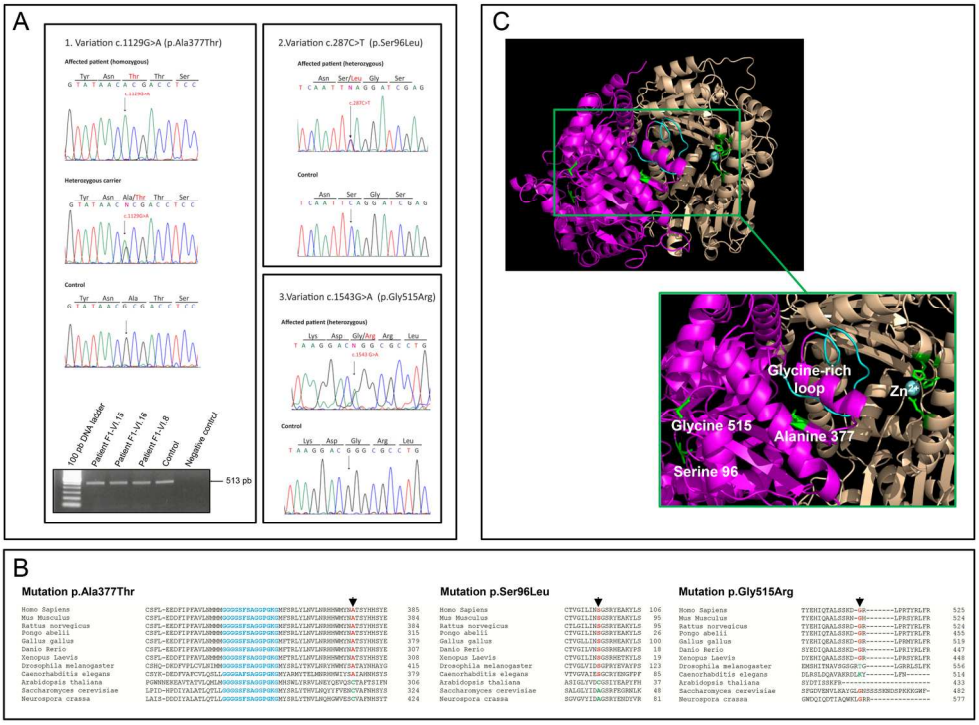

190x142mm (300 x 300 DPI)

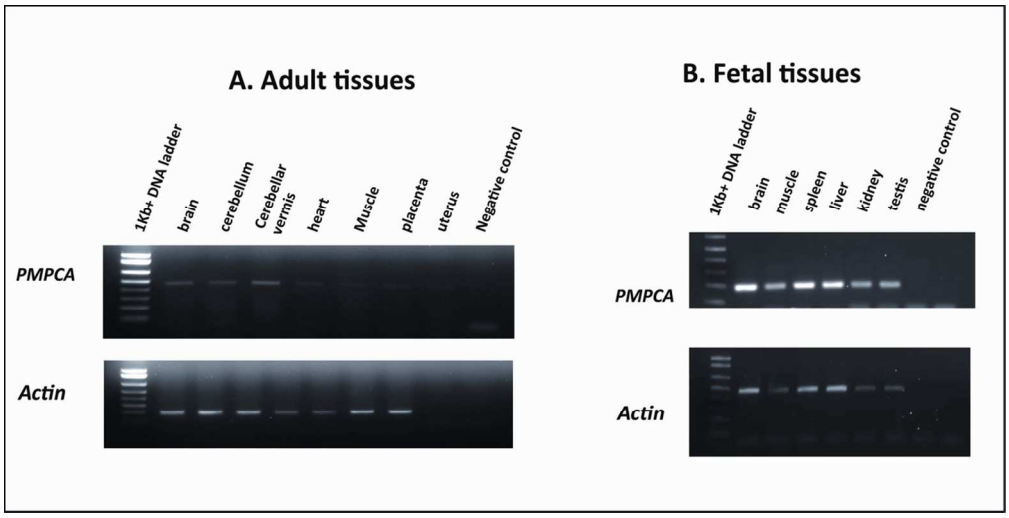

110x56mm (300 x 300 DPI)

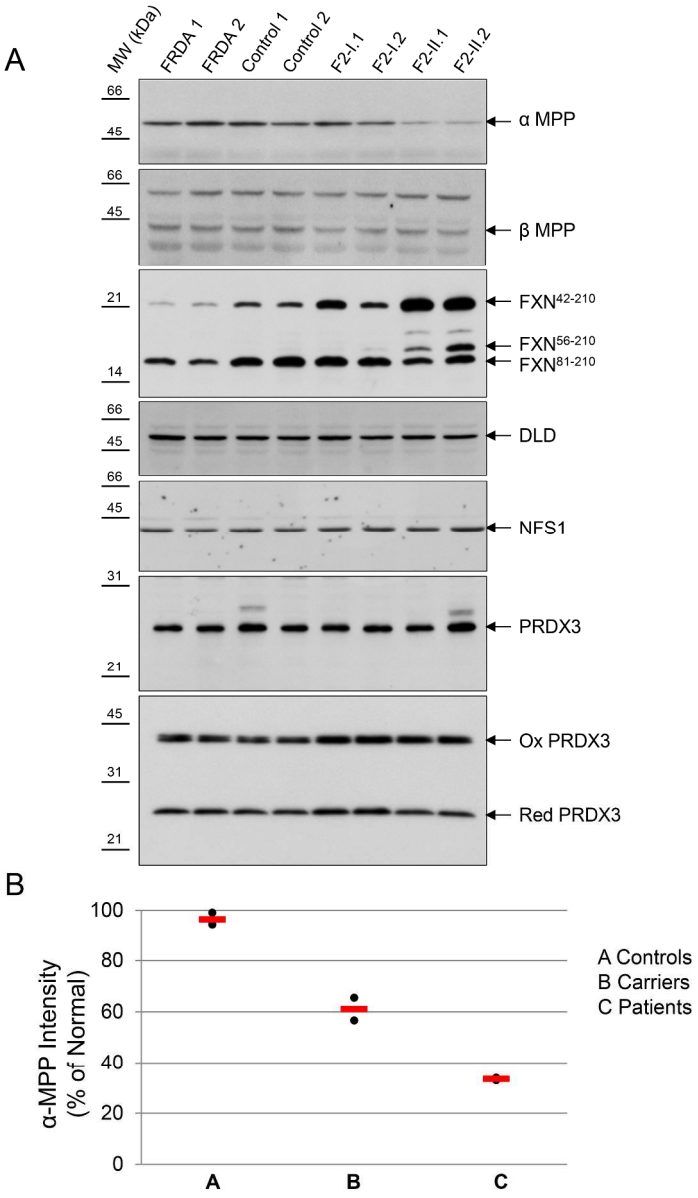

223x371mm (300 x 300 DPI)

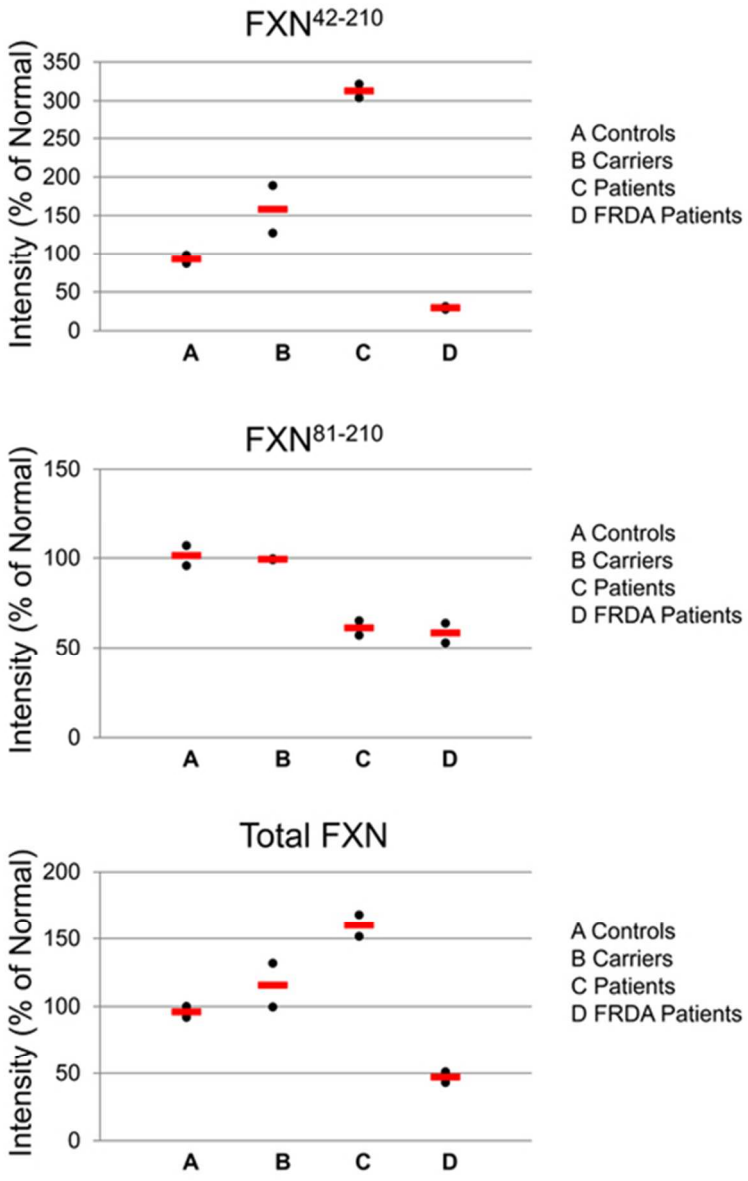

21x32mm (600 x 600 DPI)

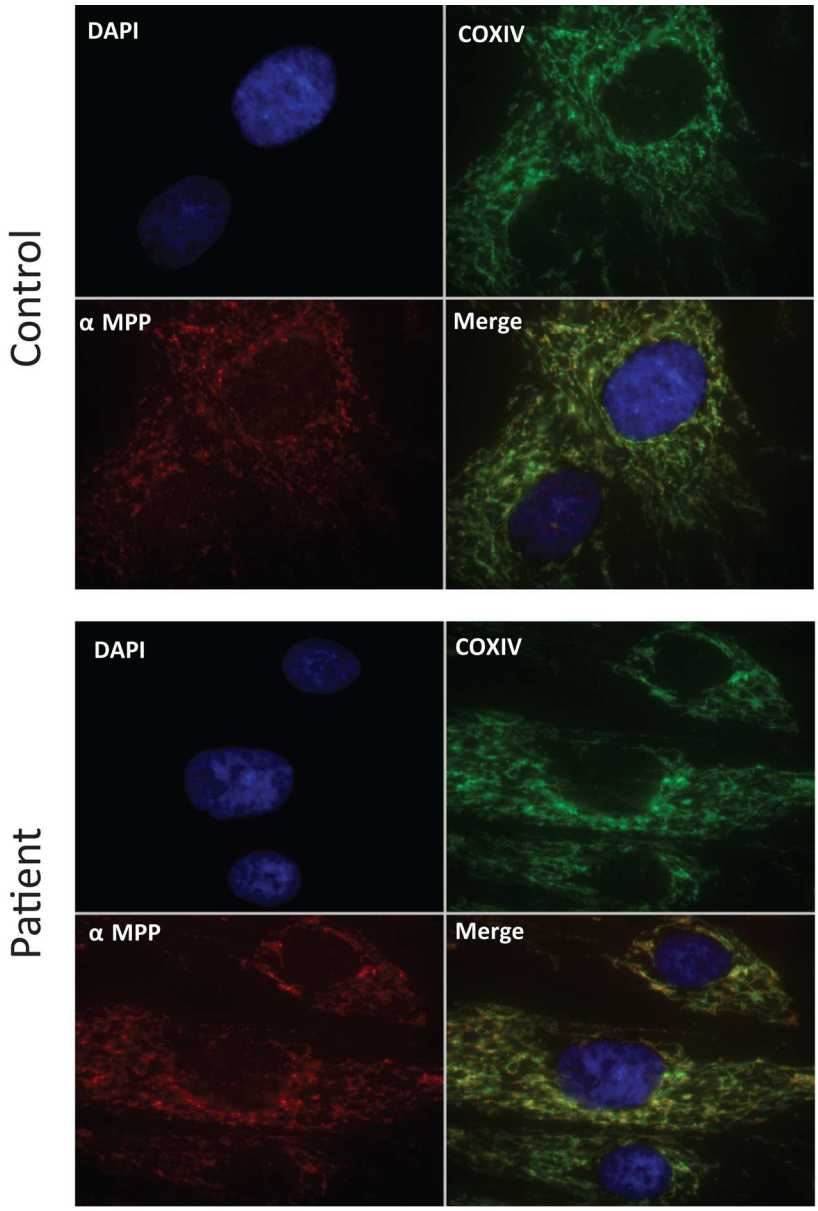

165x216mm (300 x 300 DPI)

PMPCA Mutations cause Abnormal Mitochondrial Protein Processing in Patients with Non-Progressive Cerebellar Ataxia

Rebekah K. Jobling[1†], Mirna Assoum[2,3†], Oleksandr Gakh[4], Susan Blaser[5], Julian A. Raiman[1], Cyril Mignot[6], Emmanuel Roze[7,8,9,10,11], Alexandra Dürr[7,8,9,10,12], Alexis Brice[7,8,9,10,12], Nicolas Lévy[2,3,13], Chitra Prasad[14], Tara Paton[15], Andrew D. Paterson[15], Nicole M. Roslin[15], Christian R. Marshall[15], Jean-Pierre Desvignes[2,3], Nathalie Roëckel-Trevisiol[2,3], Stephen W. Scherer[15,16], Guy A. Rouleau[17], André Mégarbané[18, §], Grazia Isaya[4§], Valérie Delague[2,3§*], Grace Yoon[1, 19§*]

Molecular Studies

SNP genotyping and CNV analysis in Family 2

To generate data for linkage analysis we genotyped 5,913 SNPs in the parents and two affected male offspring from family 2 using the Illumina HumanLinkage-24 v1.0 BeadChip (Illumina Inc., San Diego, CA, USA) according to the manufacturer's protocol. This assay uses the Infinium HD Ultra Assay where 200ng of DNA (4µL at 50ng/µL) is independently amplified, labelled, and hybridized to BeadChip microarrays then scanned with default settings using the Illumina iScan. Analysis and intra-chip normalization of resulting image files was performed using Illumina's GenomeStudio Genotyping Module software v.2011 with default parameters. Genotype calls were generated using the Illumina-provided genotype cluster definitions file (InfiniumLinkage-24_11419173_A.egt, generated using HapMap project DNA samples) with a call rate ranging from 97.8-98.7%. To obtain a higher resolution scan for copy number variation analysis we also genotyped the proband using the Infinium Human660W-Quad v1.0 BeadChip which contains 657,633 markers across the genome. Genotype calls were generated using the Illumina-provided genotype cluster definitions file (Human660W-Quad_v1_A.egt, generated using HapMap project DNA samples) with a Gencall cutoff of 0.15. Copy number variation analysis was performed using the GenomeStudio module CNV partition 3.1.6 with default cutoffs. Resulting CNVs were examined through comparison to the Database of Genomic Variants (dgv.tcag.ca). No pathogenic copy number variants known to be associated with a disease phenotype were detected.

Linkage and homozygosity mapping

Family 1

A genomewide analysis using microsatellites markers was performed as described in (Delague *et al.*, 2001).

Family 2

Following initial quality control analysis and removal of markers that did not validate, 5792 SNPs were available for linkage. Because we did not have ancestry matched controls genotyped with the linkage array we compared allele frequencies to Middle Eastern populations genotyped as part of the HGDP. From these, a set of 2613 SNPs with an average spacing of 1.5cM were extracted according to the following criteria: (1) they were on the autosomes or chromosome X, (2) they were common to the set of SNPs genotyped in the HGDP samples, and (3) they had unique positions on the genetic map. The family was analyzed using multipoint parametric linkage analysis using Merlin 1.1.2 (Abecasis *et al.*, 2002). A fully penetrant recessive model was assumed, with a disease allele frequency of 0.001. Multipoint linkage analysis resulted in a maximum LOD score of 0.602 for the nuclear family (assuming no inbreeding), which was observed on 11 different chromosomes. A total of 27 regions had maximum LOD scores >0.48 (80% of max theoretical score), spanning approximately 640 cM. Estimates of inbreeding coefficients obtained by FEstim 1.3 (Leutenegger *et al.*, 2003) suggested that although the parents are not closely related to each other, they are themselves inbred. Therefore, homozygosity mapping was also performed using FEstim 1.3 (Leutenegger *et al.*, 2006), which incorporates the inbreeding coefficient estimates into the analysis, again assuming a fully penetrant recessive model with a disease allele frequency of 0.001. This resulted in 7 regions

with LOD>1, all of which were also detected by traditional linkage analysis (Supplementary Table S3). The total length of regions identified from homozygosity mapping was 80 cM.

Whole Exome sequencing

Family 1

Exome sequencing was carried out on individual F1-VI.2 from family 1 (Fig. 1). Targeted exome sequencing, library preparation, capture and sequencing were performed by the French National Genotyping Center (CNG). Exomes were captured and enriched using the in solution Agilent SureSelect Human All Exon kit v3.0 (Sulonen *et al.*, 2011) and then sequenced on an Illumina HiSeq2000, using a paired-end 100-bp read sequencing protocol. Image analysis and base calling were performed using the Illumina Data Analysis Pipeline Software 1.5 with default parameters. Raw data were mapped to the current built of the human genome (hg19) by using BWA 0.75 (Li and Durbin, 2009) .Variant calling was subsequently performed using GATK 2.5.2 (McKenna *et al.*, 2010) and annotation was done with ANNOVAR (Wang *et al.*, 2010). In order to predict the deleterious effect of the identified sequence variations, different bioinformatics tools were applied; such as MutationTaster (http://www.mutationtaster.org/), SIFT (http://sift.bii.a-star.edu.sg/) (Kumar *et al.*, 2009), PROVEAN(http://provean.jcvi.org/index.php/) (Choi *et al.*, 2012), PolyPhen-2 (http://genetics.bwh.harvard.edu/pph2/), and UMD predictor (http://umd-predictor.eu/). In order to further refine the list of candidate nucleotide variations, additional filtering was performed on what we called the "dbSNP13700" database (i.e. dbSNP137, from which we have removed mutations that are reported as pathogenic alleles, as well as all referenced variants with frequencies lower than 1%, or without any frequency information).

Additional filtering was also performed using our in-house exome database that includes all homozygous variants detected by exome sequencing of 14 Lebanese unaffected individuals.

Family 2

Ion proton Whole Exome Sequencing was performed on patient F2-II.2, following commercially available protocols for sequencing with the Ion Proton System after enrichment with the TargetSeq Exome v1 capture process (Life Technologies Carlsbad, CA, USA) except we used the Adaptive Focused Acoustics method on a Covaris S2 instrument to shear 1µg of high quality genomic DNA to an average of 150-bp. For ligation, nick repair, purification, size selection and final amplification prior to exome capture we followed the TargetSeq v1 protocol. An aliquot of 500 ng of amplified genomic library was used in the TargetSeq Exome enrichment step. The captured library was diluted to 7 pM and amplified to obtain template-positive Ion Sphere Particles using the Ion OneTouch 2 System (Life Technologies). After enrichment, the sample was loaded onto a P1 Proton Chip and sequenced by Proton sequencers. Raw signal processing, base calling, alignment and germline (diploid) variant detection was performed using Lifetech's Torrent Server v3.6. Alignment of reads to the human genome reference hg19 (NCBI build GRCh37) was performed using Tmap 3.4.0 and single nucleotide and small insertion/deletion variant calling was done with the Torrent variant caller 3.6.

The resulting variant call file (vcf) containing SNV and indels was annotated using a combination of SNPEff (http://snpeff.sourceforge.net/) and ANNOVAR (Wang *et al.*, 2010). Variants were filtered to differentiate novel variants from known polymorphisms by screening against public single nucleotide polymorphism databases (dbSNP, http://www.ncbi.nlm.nih.gov/projects/SNP/; 1,000 genomes, www.1000genomes.org; [1000 Genomes Project Consortium *et al.*, 2010]; NHLBI Exome Sequencing Project Exome Variant

Server http://evs.gs.washington.edu/EVS/). Novel SNVs were also annotated with SIFT (Kumar *et al.*, 2009) and PolyPhen-2 (Adzhubei *et al.*, 2010) scores to predict the putative effect of the variant on protein function. We prioritized variants in the linked regions based on presumed autosomal recessive inheritance. Candidate variants were confirmed through Sanger validation in a CLIA approved laboratory (The Hospital for Sick Children) in all four members of the family.

Control Sample Genotyping Assay

We genotyped 146 Lebanese population samples for the c.1129G>A (p.Ala377Thr) mutation using a TaqMan® Custom SNP Genotyping Assay (Life Technologies Carlsbad, CA, USA). The mutant probe-2 sequence was atgtataacAcgacctcct and wild type probe-1 was atgtataacGcgacctcct. The forward primer sequence was 5' TCCAGTTTCCCATGGCCTGAT 3', and the reverse primer was 5' ATGGATGCAAAGGAGGCCAGT 3'. Sanger sequence-validated samples from patients and parents from family 2 were used as homozygous variants and heterozygous positive controls in the experiment. Genomic DNA concentration was determined using the Quant-iT™ PicoGreen® dsDNA Assay Kit (Life Technologies Carlsbad, CA, USA) and all samples were normalized to a concentration of 50 ng/µL. A master mix was prepared using 120 µL of nuclease-free water, 180 µL of TaqMan® Genotyping Master Mix and 3.5 µL of custom probe. 96-well plates were prepared with 11 µL of prepared master mix and 1 µL of DNA. After initial denaturation of 95°C for 10 min, cycling conditions were: 40 cycles at 95°C for 15 sec and 55°C for 60 sec. Post-PCR reading was performed in a ViiA™ 7 Real-Time PCR System according to standard protocols. 312 Lebanese and 186 French control individuals were screened for the c.1129G>A (p.Ala377Thr) mutation and for the c.287C>T (p.Ser96Leu)

and c.1543G>A (p.Gly515Arg) mutations, respectively, by Sanger sequencing as described below.

Capillary Sanger Sequencing

Genomic and cDNA sequences of *PMPCA* (NM_015160) were obtained from the UCSC Genomic Browser, February 2009 human reference sequence (GRCh37). Primers used for PCR amplification were designed using Primer3 software (http://frodo.wi.mit.edu) to amplify the region surrounding the mutation detected by exome sequencing in *PMPCA* exon 10 and *CAMSAP1* exon 11 (primer sequences available upon request). PCR products were purified by exonuclease I/Shrimp Alkaline Phosphatase treatment (ExoSAP-IT; Fisher Scientific SAS) according to the manufacturer's instructions and both strands were sequenced using the Big Dye® Terminator v1.1 Cycle Sequencing Kit (Applied Biosystems). Sequence reactions were purified on Sephadex G50 (Amersham Pharmacia Biotech, Foster City, CA) and capillary electrophoresis was performed on Genetic Analyser 3100 (Applied Biosystems). Electrophoregrams were analyzed on the Sequence Analysis Software version 5.2 (Applied Biosystems) and aligned with the reference sequence for *PMPCA* using ChromasPro version 1.22 (Technelysium, Queensland, Australia).

Genotyping of polymorphic markers

6 STRs and 9 SNPs flanking the *PMPCA* gene on chromosome 9q34.3 were selected. The STRs were: D9S1818 (AFMB001VE9), D9S298, D9S312, D9S67, D9S158 (AFM073YB11), D9S1838 (AFMB303ZG9), and the SNPs were: rs914397, rs61743074, rs2004074, rs11103190,

rs4604565, rs17567909, rs7869520, rs2271867. The c.2453C>T variation in *CAMSAP1* was also genotyped in all patients. All these markers span a 3.99 Mb region at 9q34.3.

PCR amplifications for STR markers were performed in a 25-µl reaction mix, containing 40 ng of genomic DNA, GoTaq® G2 Colorless Master Mix 1X (Promega, Madison, USA), containing GoTaq® G2 Hot Start Polymerase, 200µM of each dNTP and 2 mM MgCl2 (final concentration), and 0.2 µM of each primer. After an initial denaturation step of 5 min at 96°C, 35 cycles of amplification (94°C for 30 sec; 50-62°C, depending on the primer pair, for 30 sec; 72°C for 30 sec) were performed, followed by a final elongation step of 10 min at 72°C.

SNPs were genotyped by direct Sanger Sequencing of PCR amplified amplicons as described above (Supplementary Table S1).

Semi-quantitative Reverse Transcriptase PCR

Complementary DNAs (cDNA) were synthesized from commercial total RNAs extracted from different human adult (brain, cerebellum, cerebellar vermis, heart, muscle, uterus (Ambion, Applied Biosystems), placenta (Clontech) and foetal (brain, muscle, spleen, liver, kidney, testis (Clontech) tissues, using the SuperScript™ II Reverse Transcriptase (Invitrogen Life Technologies) according to the manufacturer's protocol. Sequences of *PMPCA* (NM_015160) and *ACTB* (β actine, NM_001101) were obtained from the UCSC Genomic Browser, February 2009 human reference sequence (GRCh37), and specific primers for cDNA amplification were designed through the Primer3 software as follows: PMPCA-ex8F: 5′-GGACGTTGACAGATCAGTGG-3′, PMPCA-ex12R: 5′-CAGCTTTCTGGAGCGAGTG-3′ and ACTB-F: 5′-TCCCTGGAGAAGAGCTACGA-3′, ACTB-R: 5′-AGCACTGTGTTGGCGTACAG-3′.

Modeling

Sequence alignments of α- and β-MPP sequences from different species was performed on the JustBio.com online tool resource using the program CLUSTAL 2.0.12. BLAST sequence analysis of human α- and β-MPP revealed 38% and 44% sequence identity to the respective yeast MPP subunits, suggesting that the available crystal structure of yeast MPP (1HR6) could be used to model the human MPP structure. Therefore, three-dimensional structural modelling was first carried out on the I-TASSER server, which implements multiple threading algorithms and iterative structure assembly simulations to find optimal sub-fragments within a protein structure database (PDB) (Roy *et al.*, 2010; http://zhanglab.ccmb.med.umich.edu/I-TASSER). Individual models were created for human α- and β-MPP and fitted into the structure of the yeast MPP heterodimer (1HR6) using PyMol. Validation of models obtained from iTASSER and PyMol was performed by inspecting their Ramachandran plot (Ramachandran *et al.*, 1963) and by ProQ analysis (http://www.sbc.su.se/~bjornw/ProQ/ProQ.cgi (Supplementary Table S2).

Cellular Studies

Cell culture

Lymphoblastoid cells

Immortalized lymphoblastoid cell lines for family 2 were generated from both affected patients and both carrier parents at The Centre for Applied Genomics, The Hospital for Sick Children (Toronto, Canada), and at the Center of Biological Resources (CRB TAC), from La Timone Hospital for Children (Marseille, France) for patients F1-VI.8, F1-VI.15 and F1-VI.22 from family 1. Lymphoblastoid cell lines from healthy individuals were from the Mayo Clinic

Biospecimens Accessioning Processing Laboratory (#326365 and #051310), the Coriell Cell Repository, including GM07535 (15 years old male) and AG09389 (14 years old male) and the CRB TAC (LT3961 and LT3452).

In addition, two FRDA patient lymphoblastoid cell lines were obtained from the Coriell Cell Repository (Coriell Institute for Medical Research) including GM16214 (15 years old male with onset at 9 years of age; homozygous for the GAA expansion with alleles of approximately 600 and 700 repeats) and GM16197 (14 years old male with FRDA onset at 8 ½ years of age; homozygous for the GAA expansion with alleles of approximately 760 and 830 repeats). Lymphoblast cultures were grown in RPMI 1640 with or without penicillin/streptomycin and 15% secfetal (Bovine) calf serum and transformed with Epstein-Barr virus according to standard methods. After immortalization, lymphoblastoid cells were grown in RPMI 1640 supplemented with 15% secfetal calf serum (PAA) and a mix of penicillin/streptomycin/amphotericin B and L-glutamine in a 37°C incubator stabilized at 5% CO_2.

Fibroblast cells

A primary fibroblast cell line was generated for patient F1-VI.22 from family 1 at the Center of Biological Resources (CRB TAC, Marseille, France) where samples are stored according to current regulations. Fibroblast control cell lines were obtained from the Coriell Cell Repository (Coriell Institute for Medical Research): AG08498 (1 year old male, foreskin fibroblasts) and AG07095 (2 years old male, foreskin fibroblasts). Primary human fibroblasts were cultured in Dulbecco's modified Eagle medium (DMEM) (Invitrogen, Life Technologies) supplemented with 15% fetal calf serum (PAA, GE Healthcare), penicillin/streptomycin/amphotericin B and L-glutamine in a 37°C incubator stabilized at 5% CO_2.

Antibodies used in this study

To perform western blot analysis of human MPP, purified recombinant rat α-MPP and rat β-MPP proteins (Cavadini *et al.*, 2002) were produced and used to generate two polyclonal antibodies in rabbits (MPPA #214 and MPPB #216). The mature amino-termini of the rat MPP subunits had been previously determined experimentally (Kleiber *et al.*, 1990; Paces *et al.*, 1993). In this study, amino acid residues 34-525 of human α-MPP and 46-489 of human β-MPP were predicted to comprise the mature form of the respective subunit after removal of the mitochondrial targeting signal, which was identified based on a high degree of sequence homology to the cognate rat MPP subunit (Supplementary Fig. S5A). For expression of recombinant human MPP subunits, *E. coli* strain BL21(DE3) (Novagen) was transformed with vector pET24a-PMPCA (including a PMPCA cDNA coding for amino acid residues 34-525 of α-MPP, cloned into sites *Nde*I-*Bam*HI of vector pET24a+), and vector pET24b-PMPCB (including a PMPCB cDNA coding for amino acid residues 46-489 of β-MPP, cloned into sites *Nco*I-*Bam*HI of vector pET24b+). Each subunit was independently expressed in *E. coli* as described for the rat MPP subunits (Cavadini *et al.,* 2002). On SDS/PAGE the recombinant α-MPP and β-MPP subunit run with apparent molecular masses between 45 and 66 kDa, consistent with the calculated molecular masses of ~54 and ~49 kDa, respectively, with α-MPP exhibiting a slightly higher electrophoretic mobility (Supplementary Fig. S5B), similar to native rat MPP subunits (Isaya *et al.,* 1991). The MPPA #214 and MPPB #216 antibodies were characterized via western blot analysis of total protein extracts from immortalized lymphoblastoid cells from one affected patient, one carrier parent, one patient with Friedreich ataxia and two controls (Supplementary Fig. S6A, B). Cell extracts were prepared from exponentially growing cell cultures as described previously in detail (Gakh *et al.,* 2010), and analyzed by SDS/PAGE and western blotting

alongside total protein extracts from *E. coli* cells overexpressing human α-MPP or β-MPP protein. MPPA #214 antibody recognized recombinant human α-MPP and cross-reacted weakly with recombinant human β-MPP (Supplementary Fig. S6A). A band co-migrating with recombinant human α-MPP was detected by MPPA #214 antibody in each of the human lymphoblastoid cell extracts analyzed, which was decreased in the carrier and the patient (Supplementary Fig. S6A). Conversely, MPPB #216 antibody recognized recombinant human β-MPP and cross-reacted weakly with recombinant human α-MPP (Supplementary Fig. S6B). A band co-migrating with recombinant human β-MPP was detected by MPPB #216 antibody in each of the human lymphoblastoid cell extracts analyzed (Supplementary Fig. S6B). Each antibody detected additional different cross-reacting proteins in the lymphoblastoid extracts but appeared suitable for independent detection of α-MPP and β-MPP (Supplementary Fig. S6A, B). Additional antibodies used in this study were anti-dihydrolipoamide dehydrogenase (DLD) polyclonal antibody (US Biologics), anti-cysteine desulfurase (NFS1) monoclonal antibody (MyBioSource.com), anti-FXN polyclonal antibody (PAC2518), anti-peroxiredoxin 3 (PRDX3) polyclonal antibody (Abnova). The specificity of the anti-DLD, anti-NFS1 and anti-FXN antibodies in cell extracts has been demonstrated before (Vaubel *et al.,* 2011; Gakh *et al.,* 2010). Recombinant PRDX3 was used to confirm the specificity of anti-PRDX3 antibody (Supplementary Fig. S4).

Immunoblotting

Fibroblasts were grown as described above and were then collected by trypsinization for 5 min with 0.05% Trypsin-EDTA (Invitrogen, Life Technologies), washed in phosphate buffered saline (PBS), and pelleted by centrifugation at 1000 x *g* for 10 min. Lymphoblastoid cell lines were

pelleted by centrifugation at 1000 x *g* for 5 min. Cell pellets were lysed on ice with 300 µl of lysis buffer containing triton 1% Triton X-100, 0.1% SDS, 0.15 M NaCl, sodium desoxycholate, 1 mM EDTA , 20 µM Tris–HCl, pH 7.5, and a cocktail of proteases inhibitor (Life Technologies). The lysate was passed through a 18-21 gauge needle and submitted to 4 cycles of sonication (15 sec followed by 15 second pause on ice between each sonication). After centrifugation for 10 min at 20,000 x g at 4°C, the supernatant was removed, protein concentration was measured by use of a BCA Protein Assay (Thermo Scientific™ Pierce) and samples stored at -80°C.

Just before loading on a Precast NuPage 12% Bis-Tris gels (Life technologies), 1% of reducing agent (Life technologies) was added to lysate samples containing 40 µg of proteins and the samples were boiled at 100°C for 10 min. After migration, proteins were transferred onto a nitrocellulose membrane (Thermo Scientific). The membrane was then blocked by incubation in blocking buffer for fluorescent western blotting (Tebu-Bio-Rockland MB-070) diluted in 1X PBS (Buffer A). The membrane was then incubated overnight with the primary antibodies in Buffer A and after several washings in PBS-Tween 20 (0.1%), was then incubated for 2 hours with secondary antibodies in Buffer A. After three final washings in PBS-Tween 20 (0.1%), the membranes were developed using an Odyssey Imager (Li-Cor Biosciences, Lincoln, NE). Primary antibodies were: rabbit polyclonal to PMPCA (Novus Biologicals, #NBP1-89126), rabbit polyclonal to PMPCB (Novus Biologicals, #NBP1-92120), rabbit polyclonal to FXN (Santa Cruz Biotechnology, #sc-25820), goat polyclonal to GAPDH (Santa Cruz Biotechnology, #sc-48167) and goat polyclonal to GFP (Abcam, #ab5449) diluted at 1/1000, 1/1000 , 1/200, 1/1000, 1/20000 respectively. Secondary antibodies were donkey anti-rabbit IRDye 800 (Li-Cor Biosciences), donkey anti-goat IRDye 680, diluted at 1/10000.

Western blot quantification

Cell extracts were prepared from exponentially growing cell cultures as described previously in detail (Gakh *et al.,* 2010), and analyzed by SDS/PAGE and western blotting with specific antibodies as described above. In all cases, the membrane after protein transfer was first stained with Ponceau S to confirm equal total protein loading and to mark the position of molecular weight standards, and then blotted with the appropriate antibody. For Fig. 5, one membrane was probed sequentially with antibodies against α-MPP and PRDX3; a second membrane with antibodies against β-MPP and NFS1, and a third membrane with antibodies against DLD and PRDX3. After each antibody, the membrane was stripped according to the manufacturer's protocol. For detection of oxidized (Ox) and reduced (Walker *et al.*, 2013) PRDX3, SDS/PAGE was performed in the absence of β-mercaptoethanol (Kumar *et al.*, 2009).

Densitometry measurements of α-MPP protein bands were collected from four different controls including two FRDA patients, and from the two carrier parents and the two affected patients from family 2, using Image Lab 5.0 (Bio-Rad) through three completely independent experiments, i.e. three separate sets of samples each comprising at least two controls, one or both carriers, and one or both patients that were prepared from independent cell cultures and analyzed by western blotting with MPPA #214 antibody as described above. To enable quantitative comparisons between samples analyzed on different blots, for any given set of samples the intensity of the α-MPP band of one of the controls was used as the normal reference, and the intensities of the α-MPP bands of the other controls, the carriers and the patients were expressed as percent of the normal reference.

Densitometry measurements of FXN 42-210 and FXN 81-210 protein bands were collected from the same subjects as described above through two independent experiments, i.e. two separate sets of samples that were prepared from independent cell cultures and analyzed by western blotting with PAC2518 antibody. To enable quantitative comparisons between samples analyzed on two different blots, for each set of samples the intensity of the FXN 42-210 or FXN 81-210 protein band of one of the two controls was used as the normal reference, and the intensities obtained for the second control, FRDA patients, and MPP carriers and patients were expressed as percent of the normal reference.

Immunostaining and Microscopy

At 90% confluency, fibroblast cultures were treated with 0.05% trypsin and 0.53 mM EDTA (Invitrogen LifeTechnologies), and 10^5 cells were plated on 2-well Lab Tek Chamber slides (Nalge Nunc International) and cultured in complete DMEM as described above. After 24 h of growth in a 37°C incubator stabilized at 5% CO_2, cells were washed twice in Dulbecco's PBS and were fixed in 4% paraformaldehyde. Cells were then washed for 10 min in PBS and were permeabilized with 0.5% Triton X-100 in PBS for 10 min at room temperature. After blocking for 30 min at room temperature in PBS containing 1% BSA, cells were incubated with primary antibodies diluted in the incubation solution for 3 h at room temperature. Primary antibodies used in here were: rabbit polyclonal to PMPCA (Novus Biologicalis, #NBP89126), mouse monoclonal to Cytochrome oxidase IV (CoxIV, Abcam, #ab33985), diluted, respectively, at 1/100 and 1/1000. After several washes in PBS, the slides were incubated for 1 hour with secondary antibodies diluted at 1/100 in PBS at room temperature. Secondary antibodies used are: donkey anti-rabbit Dylight R 488 (Abcam, #ab96919) and horse anti-mouse Dylight R 549

(#DI2549, Vector Laboratories). After being washed three times for 10 min in PBS, cells were incubated in 4% paraformaldehyde for 5 min and washed 10 min in PBS. Finally, after a 15 min incubation in DAPI (Sigma-Aldrich) at 100 ng/ml, the slides were mounted in Vectashield mounting medium (Vector), coverslipped, and sealed. Digitized microphotographs were recorded using an ApoTome.2 fluorescent microscope (ZEISS, Germany), equipped with an AxioCam MRm camera. Image processing was performed either with Axiovision or with ImageJ software (National Institutes of Health, MD, USA)

Supplementary References

Abecasis GR, Cherny SS, Cookson WO, Cardon LR. Merlin--rapid analysis of dense genetic maps using sparse gene flow trees. Nat Genet 2002; 30: 97–101.

Adzhubei IA, Schmidt S, Peshkin L, Ramensky VE, Gerasimova A, Bork P, et al. A method and server for predicting damaging missense mutations. Nat Methods 2010; 7: 248–249.

Delague V, Bareil C, Bouvagnet P, Salem N, Chouery E, Loiselet J, et al. A non-progressive autosomal recessive ataxia maps to chromosome 9q34-9qter in a large consanguineous Lebanese family. Ann Neurol. 2001;50:250-3.

Leutenegger A-L, Brum B, Génin E, Verny C, Lemainque A, Clerget-Darpoux F, Thompson EA. Estimation of the inbreeding coefficient through use of genomic data. Am. J. Hum. Genet. 2003; 73:516-523.

Leutenegger AL, Labalme A, Genin E, Toutain A, Steichen E, Clerget-Darpoux F, et al. Using genomic inbreeding coefficient estimates for homozygosity mapping of rare recessive traits: application to Taybi-Linder syndrome. Am J Hum Genet 2006; 79: 62–66.

Li H, Durbin R. Fast and accurate short read alignment with Burrows-Wheeler transform. Bioinformatics. 2009;25(14):1754-60.

McKenna A, Hanna M, Banks E, Sivachenko A, Cibulskis K, Kernytsky A, et al. The Genome Analysis Toolkit: a MapReduce framework for analyzing next-generation DNA sequencing data. Genome Res. 2010;20(9):1297-303.

Roy A, Kucukural A, Zhang Y. I-TASSER: a unified platform for automated protein structure and function prediction. Nature Protocols 2010; 5: 725-738.

Ramachandran GN, Ramakrishnan C, Sasisekharan V. Stereochemistry of polypeptide chain configurations. J. Mol Biol 1963; 7: 95–9.

Cavadini P, Gakh O, Isaya G. Protein import and processing reconstituted with isolated rat liver mitochondria and recombinant mitochondrial processing peptidase. Methods 2002; 26: 298-306.

Kleiber J, Kalousek F, Swaroop M., Rosenberg LE. The general mitochondrial matrix processing protease from rat liver: structural characterization of the catalytic subunit. Proc. Natl. Acad. Sci. U S A 1990; 87: 7978-82.

Paces V, Rosenberg LE, Fenton WA, Kalousek F. The beta subunit of the mitochondrial processing peptidase from rat liver: cloning and sequencing of a cDNA and comparison with a proposed family of metallopeptidases. Proc. Natl. Acad. Sci. U S A 1993;90:5355-8.

Isaya G, Kalousek F, Fenton WA, Rosenberg LE. Cleavage of precursors by the mitochondrial processing peptidase requires a compatible mature protein or an intermediate octapeptide. J. Cell. Biol. 1991;113: 65-76.

Sulonen AM, Ellonen P, Almusa H, Lepisto M, Eldfors S, Hannula S, et al. Comparison of solution-based exome capture methods for next generation sequencing. Genome Biol. 2011;12(9):R94.

Vaubel RA, Rustin P, Isaya G. Mutations in the dimer interface of dihydrolipoamide dehydrogenase promote site-specific oxidative damages in yeast and human cells. J. Biol. Chem. 2011;286: 40232-45.

Wang K, Li M, Hakonarson H. ANNOVAR: functional annotation of genetic variants from high-throughput sequencing data. Nucleic Acids Res. 2010;38:e164.

Supplementary Figures and Tables

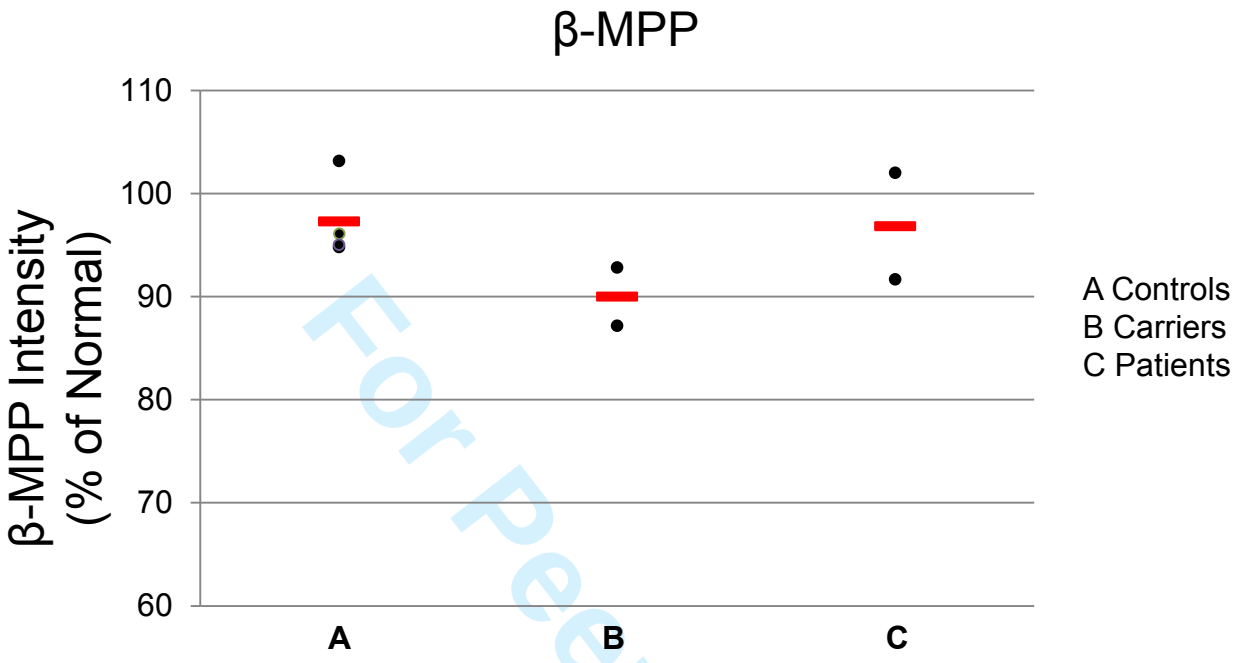

Supplementary Figure S1. Densitometry measurements of β-MPP protein bands were collected from four different controls including two FRDA patients, the two carrier parents and the two affected patients using Image Lab 5.0 (Bio-Rad) through two independent experiments, i.e. two separate sets of samples each comprising four controls, the two carriers and the two patients that were prepared from independent cell cultures and analyzed by western blotting with anti- β-MPP antibody as in Fig. 3A. To enable quantitative comparisons between samples analyzed on two different blots, for each given set of samples the intensity of the β-MPP band of one of the controls was used as the normal reference, and the intensities of the β-MPP bands of the other controls, the carriers and the patients were expressed as percent of the normal reference. The total number of β-MPP protein bands analyzed was N=2 for each control, carrier and patient. Each data point shows the mean of technical replicates for each subject in the group.

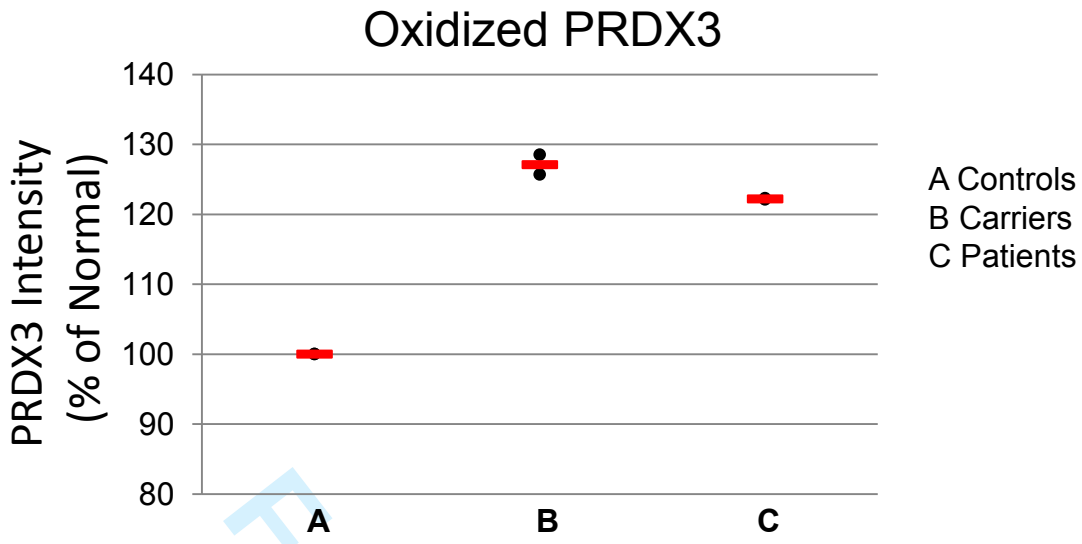

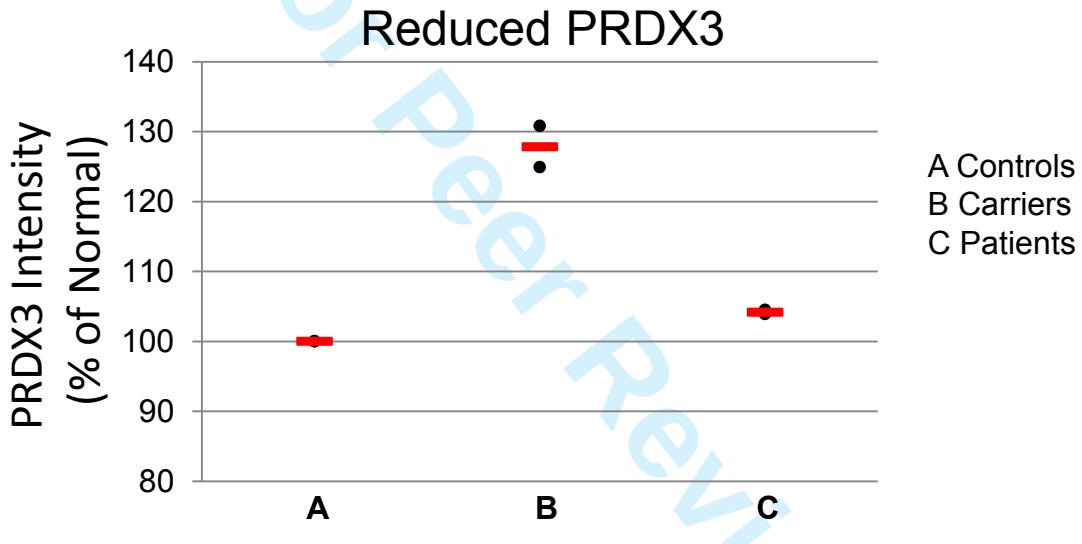

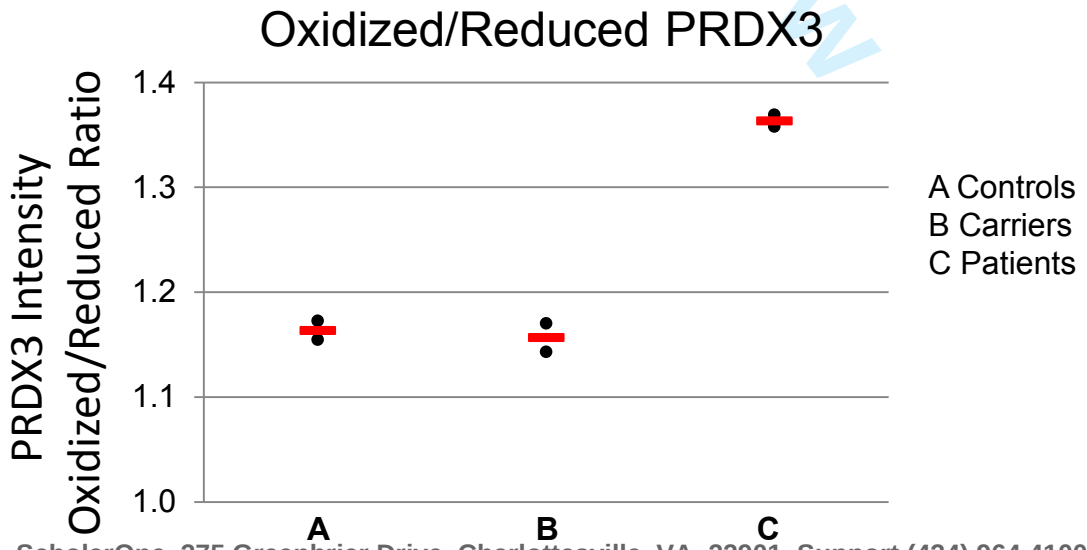

Supplementary Figure S2

Supplementary Figure S2. Densitometry data were obtained from two controls, and from the two carrier parents and the two affected patients from family 2. Cells were treated with N-Ethylmaleimide in all steps of processing, from harvesting to protein extraction, to prevent non-specific oxidation of PRDX3 (Kumar et al. 2009). The 6 samples were separated on 15% SDS-PAGE in the absence of β-mercaptoethanol, transferred to membrane and blotted with antibodies against PRDX3. The intensity of the PRDX3 oxidized or reduced band measured in one of the two controls was used as the normal reference. The intensities measured in the other control, the carriers and the patients were expressed as percent of normal. Data points show the measurements performed for each of the three groups, and the red line shows the mean. Data analysis was performed using Image Lab 5.0 (Bio-Rad).

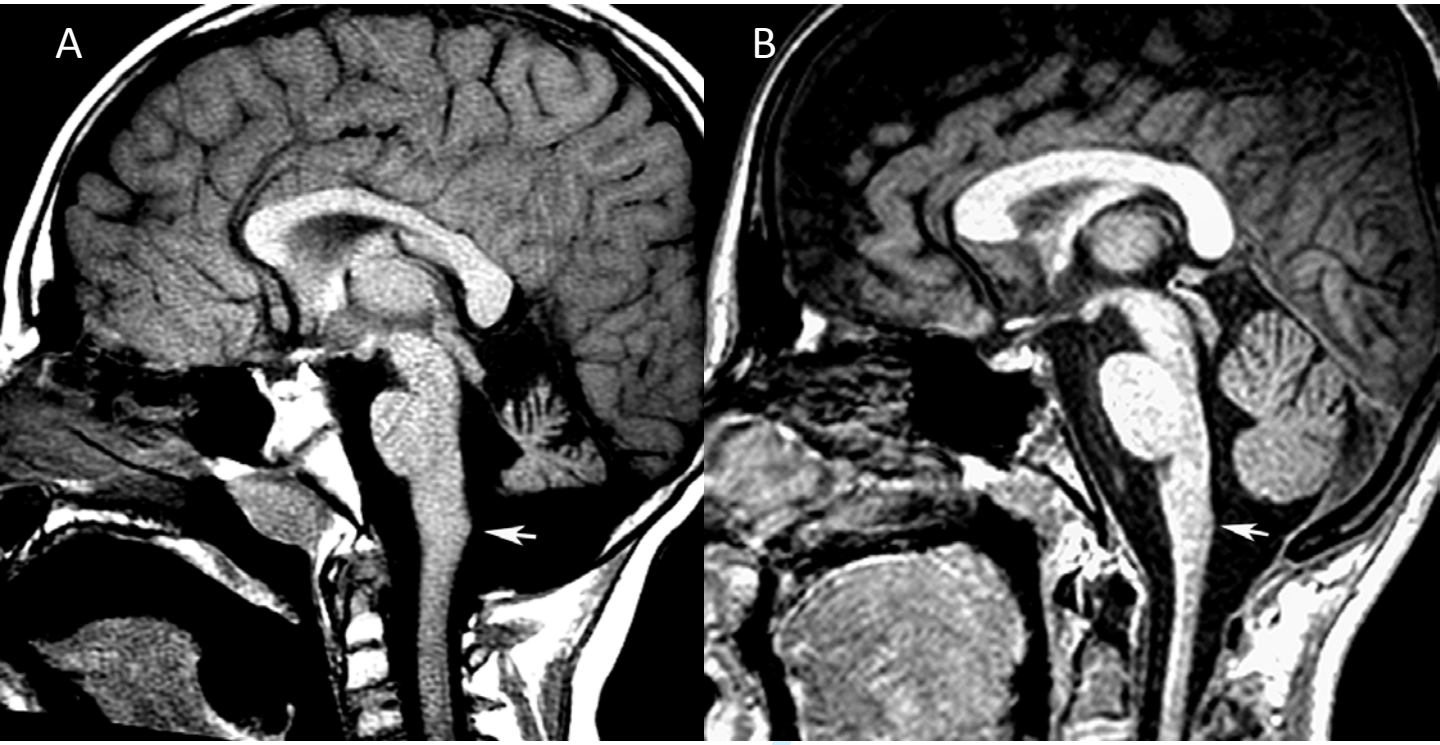

Supplementary Figure S3. Comparison between imaging in (A) PMPCA and (B) FRDA.

In Friedreich ataxia (B), there is volume loss in the dentate nuclei, dorsal root ganglia and gracile and cuneate nuclei with resultant thinning of afferent fibres. Cerebellar atrophy is mild, but confirmed on volumetric studies. On sagittal images, the clava (location of gracile and cuneate nuclei) (arrows) in FRDA is small in comparison to that in PMPCA (A). Additionally, the upper cervical cord is slender in FRDA. The vermis is normal in size and configuration in FRDA (B), while there is considerable loss of vermian volume in PMPCA (A).

Brain

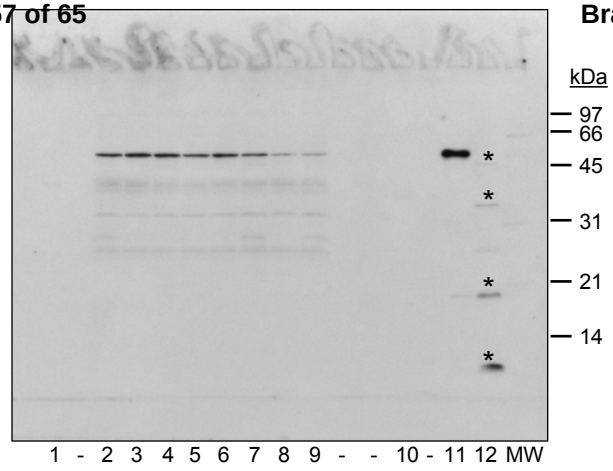

Membrane #1 probed with anti-α-MPP antibody

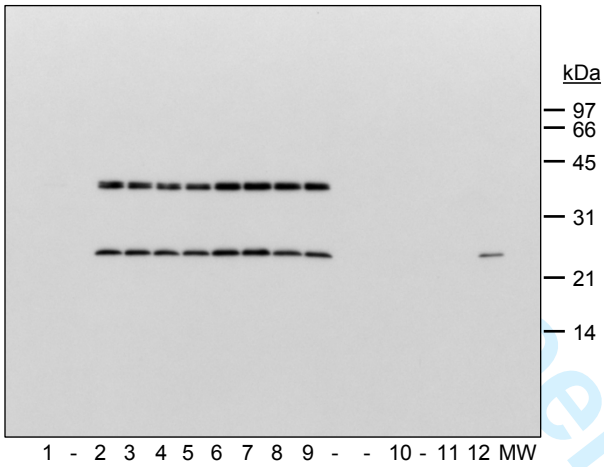

Membrane #1 probed with anti-PRDX3 antibody
2 sec exposure

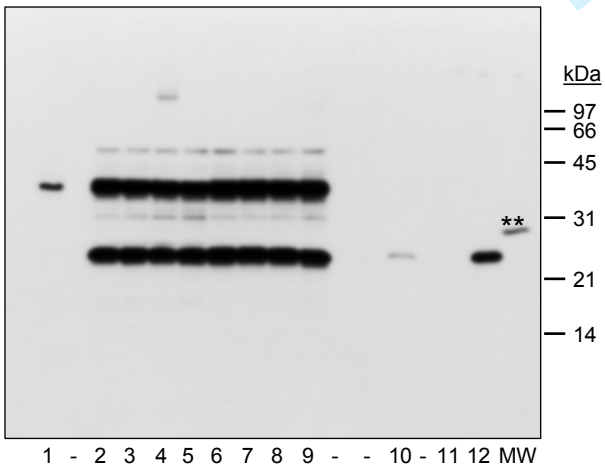

Membrane #1 probed with anti-PRDX3 antibody
5 min exposure

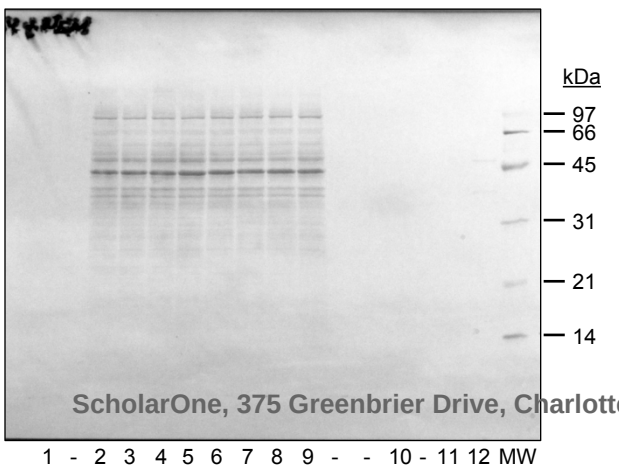

Membrane #1 stained with Coomassie

Supplementary Figure S4, A

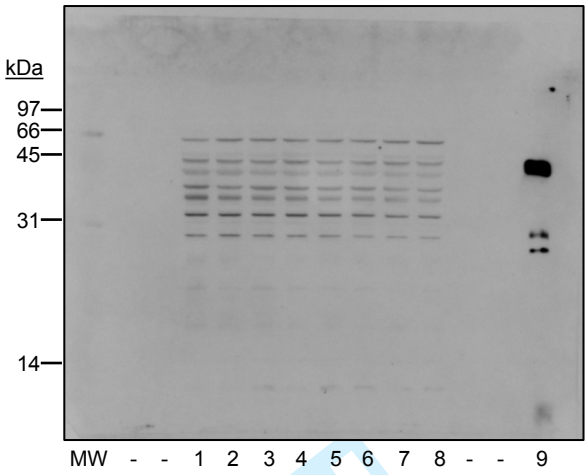

Membrane #2 probed with anti β-MPP antibody

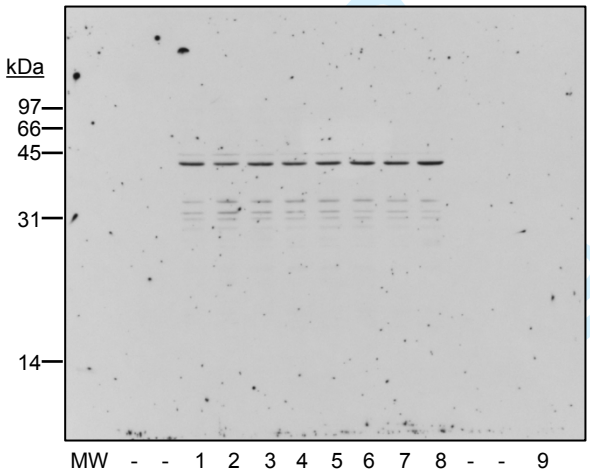

Membrane #2 probed with anti-NFS1 antibody

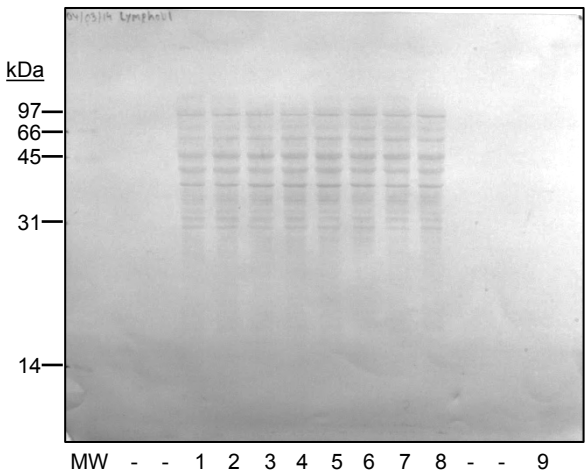

Membrane #1 stained with Coomassie

Supplementary Figure S4, B

Brain

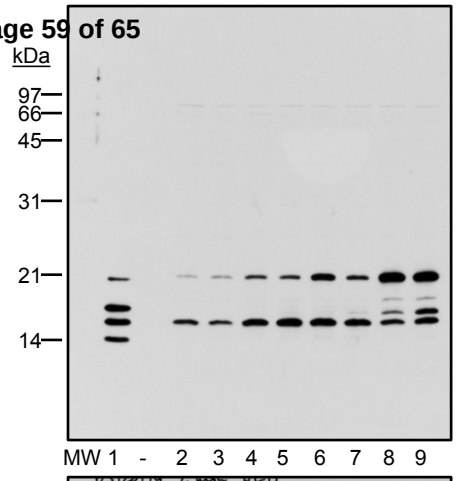

Membrane #3 probed with anti-FXN antibody

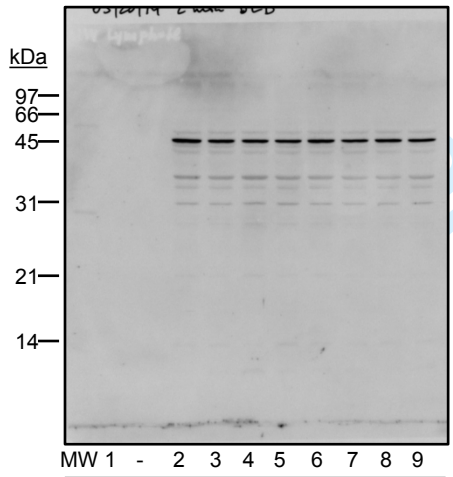

Membrane #3 probed with anti-DLD antibody

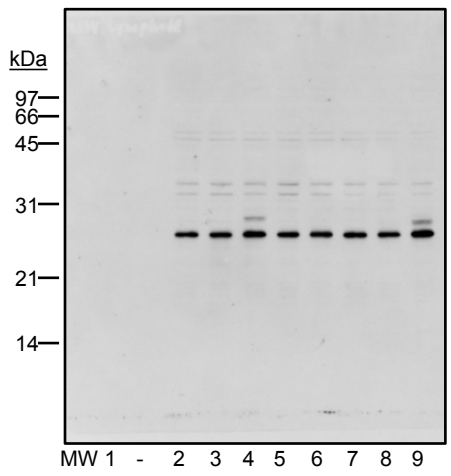

Membrane #3 probed with anti-PRDX3 antibody

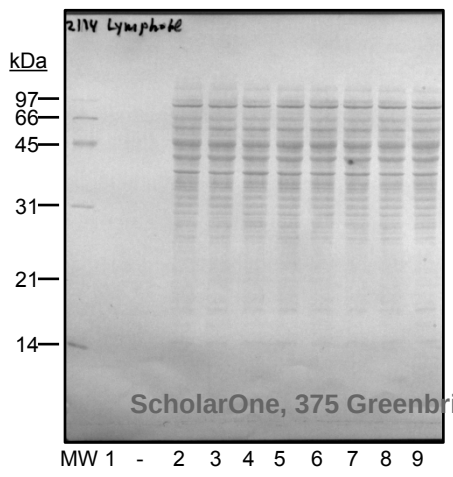

Membrane #3 stained with Coomassie

Supplementary Figure S4, C

Supplementary Figure S4. Full-length versions of the cropped blots shown in Fig. 3.
(**A**) Membrane #1 was probed sequentially with antibodies against α-MPP and PRDX3. After each antibody, the membrane was stripped per manufacturer's protocol. At the end, the membrane was stained with Coomassie Brilliant Blue R-250 (Coomassie). Lanes 2-9, lymphoblastoid cell extracts; lane 1 and lane 10: purified recombinant PRDX3 in oxidized (- β-mercaptoethanol) and reduced (+ β-mercaptoethanol) form, respectively, which are detected after a 5 min exposure; lane 11: extract of *E. coli* cells expressing recombinant α-MPP; lane 12: extract of *E. coli* cells expressing recombinant β-MPP plus purified recombinant PRDX3 in reduced form (3 fold more protein compared to lane 10). –, empty lane; *, full-length recombinant β-MPP and degradation products of the protein, with which the anti α-MPP antibody cross-reacts weakly, as shown in Supplementary Fig. 6A; **, weak reactivity of anti-PRDX3 antibody with one of the MW markers.
(**B**) Membrane #2 was probed sequentially with antibodies against β-MPP and NFS1. After each antibody, the membrane was stripped per manufacturer's protocol. At the end, the membrane was stained with Coomassie Brilliant Blue R-250 (Coomassie). Lanes 1-8, lymphoblastoid cell extracts; lane 9: extract of *E. coli* cells expressing recombinant β-MPP. –, empty lane.
(**C**) Membrane #3 was probed sequentially with antibodies against FXN, DLD, and PRDX3. After each antibody, the membrane was stripped per manufacturer's protocol. At the end, the membrane was stained with Coomassie Brilliant Blue R-250 (Coomassie). Lanes 2-9, lymphoblastoid cell extracts; lane 1: purified recombinant FXN isoforms. –, empty lane.

A

```
                                                  34
Human α-MPP MAAVVLAATRLLRGSGSWGCSRLRFGPPAYRRFSSGGAYPNIPLSSPLPGVPKPVFATVD  60
            MA  V AA RLLRGS +  C+R +FG PA+RRFSSG  YPNIPLSSPLPGVPKP+FATVD
Rat   α-MPP MATAVWAAARLLRGSAAL-CARPKFGSPAHRRFSSGATYPNIPLSSPLPGVPKPIFATVD  59

                                                                  46
Human β-MPP MAAAAARVVLSSAARRRLWGFSESLLIRGAAGRSLYFGENRLRSTQAATQVVLNVPETRV  60
            MAAAA    L   A RRLWGF+  L +R AA + LYFG +RLRSTQAA QVVLNVPET+V
Rat   β-MPP MAAAAVSRTLLPVAGRRLWGFTRRLPLRAAAAQPLYFGGDRLRSTQAAPQVVLNVPETQV  60
```

B

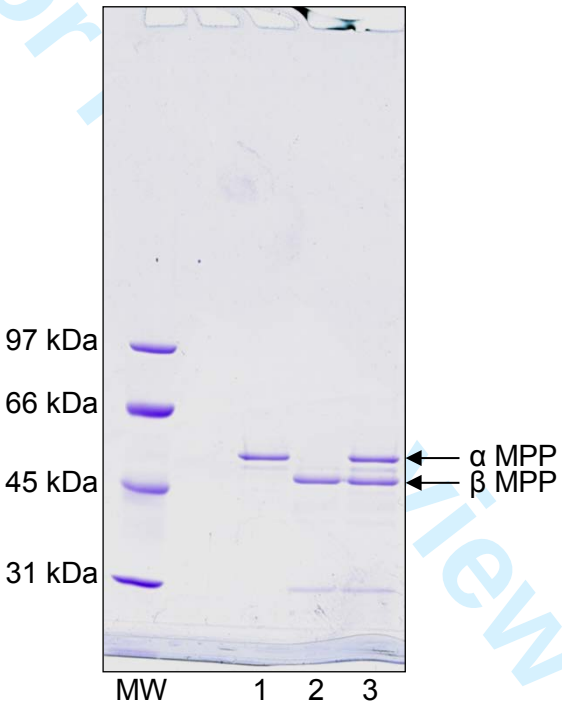

Supplementary Figure S5. (**A**) The amino-terminal sequences of the human and rat α-MPP and β-MPP precursor polypeptides were aligned using the program CLUSTAL 2.0.12 on the JustBio.com online tools resource. The mature amino-termini of the rat MPP subunits were determined experimentally (Kleiber et al. 1990; Paces et al. 1993), and were used in this study to define the mature amino-termini of the human MPP subunits. Rat and human leader peptides are highlighted in red and blue respectively, and the mature protein amino-termini (Serine 34 and Glutamine 46) are in bold. (**B**) Recombinant α-MPP and β-MPP proteins expressed in *E. coli* migrate on 12% SDS-PAGE with apparent molecular masses between 66 and 45 kDa, consistent with their calculated molecular masses of 54 and 49 kDa, respectively. Protein bands were detected by staining with Coomassie Brilliant Blue. Total length of gel is shown.

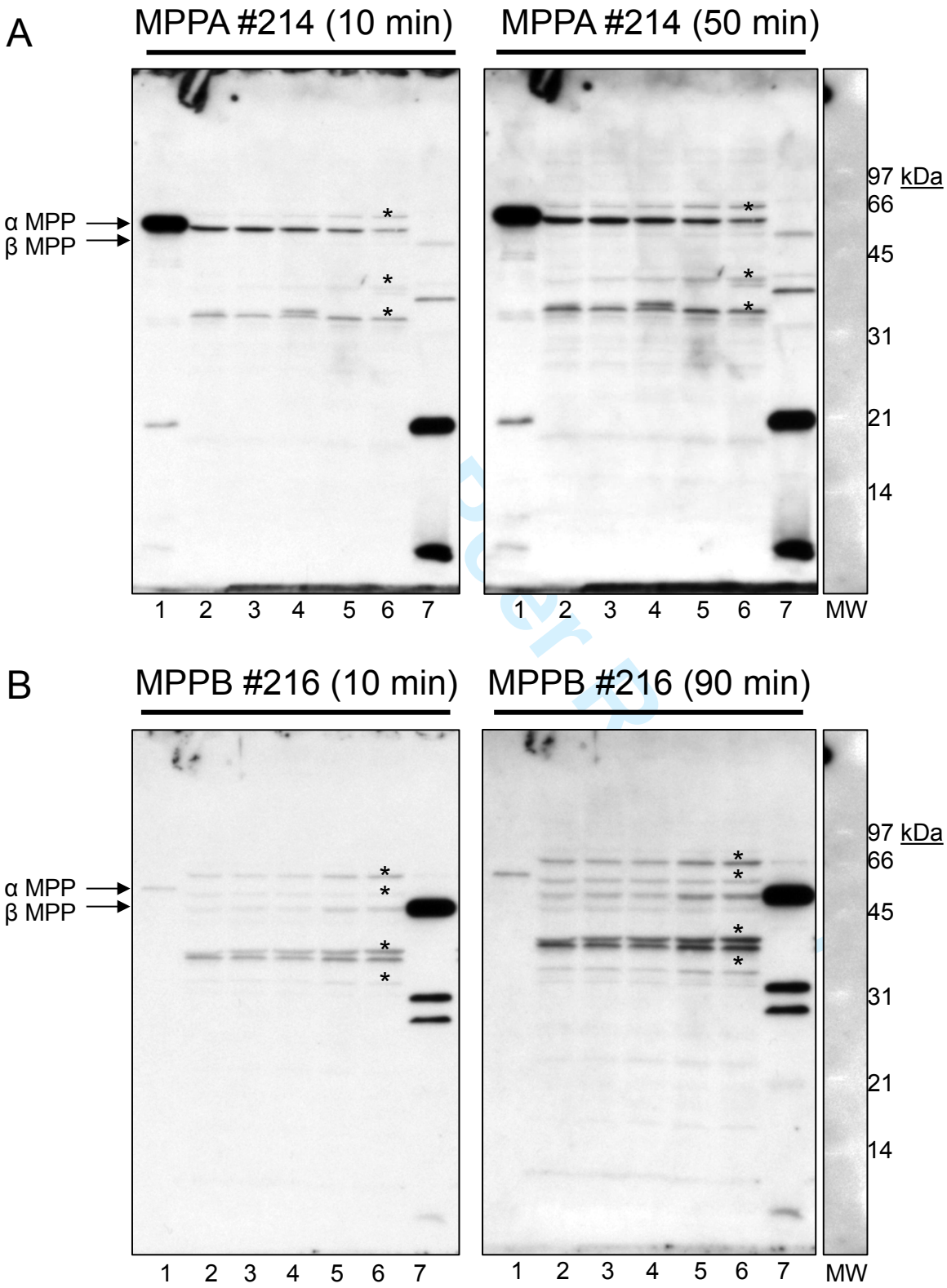

Supplementary Figure S6

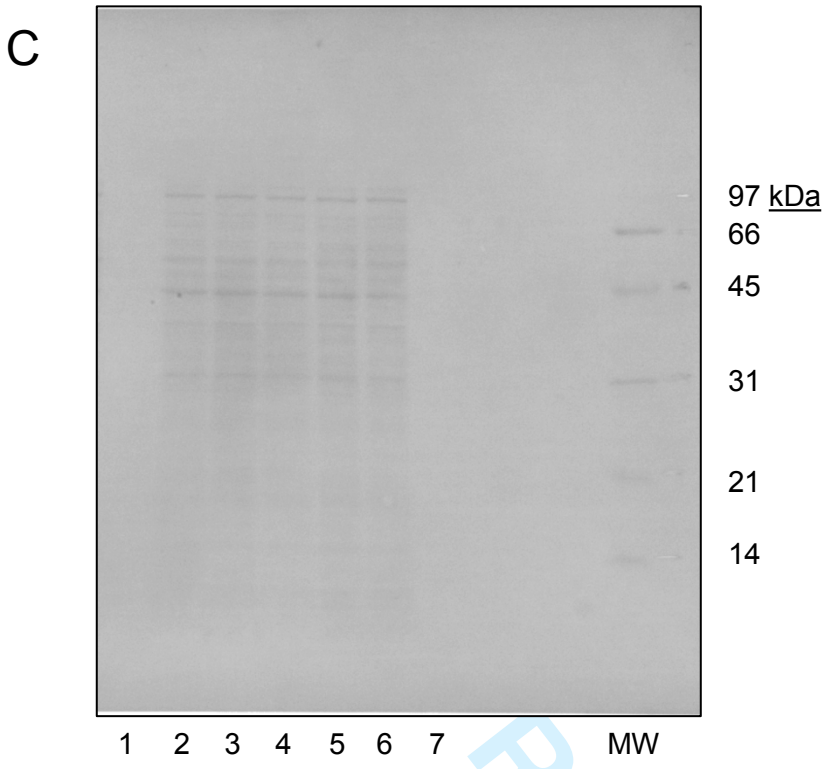

Supplementary Figure S6. Total protein extracts from immortalized lymphoblastoid cells (GM 16214 FRDA, GM07535 Normal, AG09398 Normal, carrier parent, affected patient; lanes 2-6) and *E. coli* cells expressing recombinant α-MPP (lane 1) or β-MPP (lane 7) were separated on 14% SDS-PAGE. After protein transfer, the membrane was stained with Ponceau S to detect the molecular weight (MW) markers, the position of which was marked with ink on the membrane (MW). The membrane was then sequentially probed with (**A**) anti α-MPP antibody (MPPA #214) followed by (**B**) anti β-MPP antibody (MPPB #216), with stripping of the membrane per manufacturer's protocol between antibodies. Upon incubation with ECL Plus Western Blotting Detection Reagents, the membrane was exposed to film for different lengths of time. Shown are two different exposures for lanes 1-7 and 90 min exposure for MW markers. Asterisks denote non-specific cross-reacting bands. The entire length of each blot is shown. The intensity of the β-MPP band is higher in the carrier band the patient compared to controls (lanes 5-6 vs. 2-4. However, this was not confirmed in subsequent western blots (Fig. 3A ad data not shown). (**C**) After western blotting, the membrane was stained with Coomassie Brilliant Blue R-250 to demonstrate equal total protein loading and MW standards. Under these conditions, the total protein in the *E. coli* extracts loaded in lanes 1 and 7 is under the limit for detection. The entire length of the membrane is shown.

Supplementary Figure S6 (cont.)

Markers	Distance between markers (kb)	Genomic coordinates (hg19)	F1-VI.2		F1-VI.4		F1-VI.8		F1-VI.9		F1-VI.10		F1-VI.15		F1-VI.16		F1-VI.17		F1-VI.18		F1-VI.21		F1-VI.22		F1-VI.24		F2-II.1		F2-II.2		F3-V.2		F3-V.5	
D9S1818		137,135,350	1	1	1	1	1	1	1	1	1	1	1	1	1	1	1	1	1	1	1	1	1	1	1	1	2	1	2	1	1	2	1	2
D9S298	372	137,507,362	1	2	2	1	1	1	1	1	1	1	1	1	1	1	1	1	1	1	1	1	1	1	1	1	1	1	1	1	1	1	1	1
D9S312	412	137,919,496	4	5	1	4	1	1	1	1	1	1	1	1	1	1	1	1	1	1	1	1	1	1	1	1	3	3	3	3	1	1	1	1
rs914397	316	138,235,962	G	G	G	G	G	G	G	G	G	G	G	G	G	G	G	G	G	G	G	G	G	G	G	G	G	G	G	G	G	G	G	G
D9S67	49.5	138,285,463	4	3	4	4	4	4	4	4	4	4	4	4	4	4	4	4	4	4	4	4	4	4	4	4	1	1	1	1	4	4	4	4
rs61743074	91.6	138,377,051	C	T	C	C	C	C	C	C	C	C	C	C	C	C	C	C	C	C	C	C	/	/	C	C	C	C	C	C	C	C	C	C
rs2004074	552	138,377,603	G	A	G	G	G	G	G	G	G	G	G	G	G	G	G	G	G	G	G	G	G	G	G	G	G	G	G	G	G	G	G	G
rs11103190	302	138,679,895	C	C	C	C	C	C	C	C	/	/	C	C	C	C	C	C	C	C	C	C	/	/	C	C	C	C	T	T	T	T	C	C	C	C
CAMSAP1 c.2453C>T (p.Ala818Val)	20.4	138,700,333	T	T	T	T	T	T	T	T	T	T	T	T	T	T	T	T	T	T	T	T	T	T	T	T	T	T	C	C	C	C	T	T	T	T
D9S158	398	139,099,048	1	1	1	1	1	1	1	1	1	1	1	1	1	1	1	1	1	1	1	1	1	1	1	1	1	1	1	1	1	1	1	1
***PMPCA* c.1129G>A (p.Ala377Thr)**	**214**	**139,313,299**	A	A	A	A	A	A	A	A	A	A	A	A	A	A	A	A	A	A	A	A	A	A	A	A	A	A	A	A	A	A	A	A
rs4604565	104	139,313,403	G	G	G	G	G	G	G	G	G	G	G	G	G	G	G	G	G	G	G	G	G	G	G	G	G	G	G	G	G	G	G	G
rs17567909	55.8	139,369,212	A	A	A	A	A	A	A	A	A	A	A	A	A	A	A	A	A	A	A	A	A	A	A	A	A	A	A	A	A	A	A	A
rs7869520	575.8	139,945,051	C	C	C	C	C	C	C	C	C	C	C	C	C	C	C	C	C	C	C	C	C	C	C	C	C	C	C	C	C	C	C	C
rs2271867	1.75	139,946,804	C	C	C	C	C	C	C	C	C	C	C	C	C	C	C	C	C	C	C	C	C	C	C	C	C	C	C	C	C	C	C	C
D9S1838	690	140,636,699	4	4	4	4	4	4	4	4	4	4	4	4	4	4	4	4	4	4	4	4	4	4	4	4	4	4	4	4	4	4	4	4

Supplementary Table S1. STRs and SNPs haplotypes for the 16 Lebanese affected individuals from families F1, F2 and F3 Patients are labeled according to the pedigrees represented in Figure 1 (each family is indicated by a color: red (F1), blue (F2) and purple (F3)). Markers are reported from centromere (top) to telomere (bottom). Genomic coordinates (hg19 built) are provided for each marker and physical distances between markers are given in Mb. The c.1129G>A (p.Ala377Thr) mutation in PMPCA is indicated in red. Accession numbers for PMPCA and CAMSAP1 are NM_015160 and NM_015447 respectively. Accession numbers for SNPs s are from the dbSNP database. Homozygous markers are marked in bold. Ancestral haplotype is drawn in orange. Comparison of haplotypes shows that a recombination occurred a long time ago in family F2, leading to a different haplotype in the proximal part of the Homozygous by Descent locus (colored in blue). The smallest common homozygous ancestral mutant haplotype shared by all patients is boxed.

Validation	Yeast MPP (1HR6)	Human α-MPP	Human β-MPP	Human MPP
Ramachandran plot[1]				
Favored region	96.7 %	87.6 %	92.3 %	89.8 %
Allowed region	2.7 %	8.8 %	5.2 %	7.1 %
Outlier region	0.4 %	3.7 %	2.5 %	3.1 %
ProQ				
Predicted LG score[2]	6.21	4.56	5.28	4.95
Predicted MaxSub[3]	0.54	0.40	0.48	0.45
Verify 3D	96.0 %	79.8 %	90.1 %	87.3 %

[1]% amino acids in favored region + % amino acids in allowed region ≥90%: model has good stereochemical quality.
[2]LGscore >1.5: fairly good model; >2.5: very good model; >4: extremely good model.
[3]MaxSub >0.1: fairly good model; >0.5: very good model; >0.8: extremely good model.
http://www.sbc.su.se/~bjornw/ProQ/ProQ.cgi

Chr	Max LOD[1]	Start			End		
		SNP	cM[2]	bp[3]	SNP	cM	bp
8	1.23	rs1016667	4.35	2,578,091	rs433960	21.74	8,768,319
9	1.22	rs4641145	154.79	137,919,491	rs7860423[4]	159.95	140,955,547
16	1.26	rs205162	49.58	25,596,637	rs4887606	57.07	34,945,227
18	1.43	rs872906	39.86	13,377,699	rs1426311	54.20	28,898,567
18	1.12	rs1943664	102.17	70,538,889	rs999647	108.45	72,571,550
22	2.07	rs11089263[5]	0	17,087,656	rs140390	12.72	21,460,008
22	1.29	rs2012607	16.02	23,285,252	rs5762174	30.28	27,865,344

[1] Regions with homozygosity LOD scores >1, under a fully penetrant recessive model with a disease allele frequency of 0.001
[2] cM positions are based on the deCODE map
[3] bp positions are from hg19
[4] Last analyzed marker on the chromosome
[5] First analyzed marker on the chromosome

Supplementary Table S3